Studies on the Chromosomal Heterogeneity Derived from Tetraploid Tumor Cells and the Influence of the Heterogeneity on the Drug Efficacy

January 2021

Sei UMEDA (SHU)

Studies on the Chromosomal Heterogeneity Derived from Tetraploid Tumor Cells and the Influence of the Heterogeneity on the Drug Efficacy

A Dissertation Submitted to
the Graduate School of Science and Technology,
University of Tsukuba
in Partial Fulfillment of Requirements
for the Degree of Doctor of Philosophy in Science

Doctoral Program in Biology

Degree Programs in Life and Earth Sciences

Sei UMEDA (SHU)

Abbreviations

BSA	bovine serum albumin
CIN	chromosomal instability
DAPI	4,6-diamidino-2-phenylindole
DI	DNA index
DMSO	dimethylsulfoxide
EGFR	epidermal growth factor receptor
FBS	foetal bovine serum
FISH	fluorescence in situ hybridization
gRNA	guide RNA
HER2	human epidermal growth factor receptor 2
IHC	immunohistochemistry
LSC	laser-scanning cytometry
HGFR/MET	hepatocyte growth factor receptor
NA	numerical aperture
PBS	phosphate-buffered saline
RTKs	receptor tyrosine kinases

SAC	spindle assembly checkpoint
STLC	S-trityl-*L*-cysteine
T-DM1	trastuzumab emtansine
ToGA	trastuzumab for gastric cancer

Table of Contents

Abstract

Chromosomal instability is one of the most prominent features of tumor cells, and it causes aneuploidy and heterogeneity. Heterogeneity contributes to drug resistance in tumors. In chapter 1, I focused on the tetraploidy as an intermediate of aneuploidy. Although a number of studies have shown the importance of tetraploidy in cancer development, how tetraploid cells transform into aneuploid cells is poorly understood. Here, I show that spindle polarity (e.g., bipolarity or multipolarity) in tetraploid cells depends on the level of functional phospho-Eg5, a mitotic kinesin, localised at the spindles. Tetraploid cells with high levels of functional Eg5 give rise to a heterogeneous aneuploid population via multipolar division. This process is suppressed by inhibition of Eg5 or expression of a non-phosphorylatable Eg5 mutant, as well as by changing the balance between opposing forces required for centrosome separation. Furthermore, Eg5 expression levels correlate with ploidy status in gastric cancer specimens. In chapter 2, to speculate the influence of heterogeneity on acquired drug resistance, I assessed the treatment-induced changes to a treatment targeted molecule (human epidermal growth factor receptor 2: HER2) using highly heterogeneous gastric cancer specimens. I analysed 6 paired pre- and post-treatment samples, and found that in 5 cases, HER2 overexpressed tumor cells were lost after treatment, and that includes both anti-HER2 treatment and cytotoxic chemotherapy. The loss of HER2 expressed cells could cause the resistance to subsequent anti-HER2 therapies. Collectively, highly Eg5 expressed tetraploid cancer

cells can accelerate the generation of aneuploidy and heterogeneity. Heterogeneous tumors can acquire resistance to targeted therapies by inducing the loss of target molecules, such as HER2.

General Introduction

One of the most prominent features of tumor cells is chromosomal instability (CIN). CIN represents the loss of chromosome segregation fidelity in mitosis, and various types of tumor cells show a high rate of chromosome missegregation during cell division, which results in aneuploid cells [1, 2]. Aneuploid cancer cells have abnormal number of chromosomes, which is highly variable, ranging from nearly haploid (1N) to more than tetraploid (4N) (Fig. 1) [3, 4]. In addition, CIN contributes to tumor heterogeneity, which drives resistance to molecularly targeted therapies [5, 6]. For example, approximately half of gastric cancers are categorised as the CIN subtype based on the gene expression [2], leading to the highly heterogeneous expression of some onco-proteins and subsequent resistance to targeted therapy [7].

There are a number of studies that propose mechanisms of generating aneuploidy cancer cells that involve an incorrect mitotic process, including dysfunction of spindle assembly checkpoint (SAC), cohesion defects, supernumerary centrosomes, and aberrant kinetochore-microtubule attachment dynamics. However, since many cancer cells contain large-scale changes in chromosome numbers, but rarely have simple gains or losses of individual chromosomes, the cause of aneuploidy cannot be sufficiently explained by repeated accumulation of mitotic errors in each mitotic process. The tetraploid intermediate model is an appealing alternative way to explain the route to aneuploidy. Some observations support the tetraploid intermediate model: tetraploid

cells can be found in some early stage tumors; and the number of chromosomes in tumor cells is frequently very high.

As a consequence of CIN, tumors gain a heterogeneous aneuploidy population made up of cells with various genomic backgrounds. This heterogeneity has been suggested to be a mechanism of resistance to anti-tumor therapies. I can indirectly assess the influence of heterogeneity on acquired drug resistance by focusing on the difference between drug responses in gastric and breast cancer. Gastric cancer is one of the most highly heterogeneous cancers; almost half of all gastric cancers are categorized as the CIN subtype according to gene expression [2]. Gastric cancer and breast cancer share the same molecular target of therapy: human epidermal growth factor receptor 2 (HER2). Anti-HER2 therapy is the standard for both HER2-positive gastric and breast cancer. HER2 expression is highly heterogeneous in intra-tumoral gastric cancer specimens, in contrast, breast cancer has more homogeneous HER2 expression patterns [8, 9].

In this study, I aimed to elucidate the molecular mechanisms by which tetraploid cells generate a heterogeneous aneuploid population, and investigate the influences of heterogeneity on anti-tumor therapies.

In the chapter 1, I focused on the mitosis of tetraploid cancer cells to reveal the mechanism of development of tetraploid cells into aneuploid cells. Tetraploid cells can arise by several mechanisms: cell fusion, mitotic slippage, and a failure to undergo

cytokinesis (Fig. 2). Cell fusion can be triggered by a viral infection, not limited to oncogenic viruses [10]. Mitotic slippage, a state where cells exit mitosis without undergoing anaphase or cytokinesis, can be caused by a SAC defect or some anti-cancer agents [11]. Cytokinesis failure can be induced by any defect in cytokinetic proteins. In addition, errors in chromosome segregation, wherein a chromosome will be left in cleavage furrow, will prevent cytokinesis and lead to tetraploidy [12]. Several lines of evidence also suggest that cytokinesis failure could be induced in response to DNA damage [13]. The most direct experimental evidence on the tumorigenesis of tetraploid cells showed that tetraploid cells, which were generated by inducing cytokinesis failure, can initiate tumor formation in a xenograft mouse model; however, diploid cells that underwent an identical procedure did not form tumors [14]. In clinical settings, tetraploid cells can be found in a pre-malignant condition called Barrett's esophagus and in the early stages of cervical carcinogenesis, and tetraploid cells predispose pre-malignant cells to the formation of aneuploidy and tumors [15, 16].

Despite the importance of tetraploid cells as an intermediate to aneuploidy, the process of progression to aneuploidy and the mitotic regulation mechanisms of tetraploid cells remain elusive. Using highly synchronised tetraploid cells, I found that the balance of forces generated by kinesins, especially mitotic kinesin Eg5 (also known as KIF11 or kinesin-5), plays an important role in determining spindle polarity (e.g., multipolarity

vs. bipolarity) in tetraploid cells. I demonstrate that spindle multipolarity and subsequent cell behaviour in tetraploid cells are determined by the level of functional Eg5 localised at the spindle, which ranges variously among cell lines. In addition, the high levels of Eg5 expression were associated with increased aneuploidy in a clinical context by examining gastric cancer specimens. Consequently, Eg5 accelerates the transition of tetraploid cells into heterogenous aneuploid cells.

In chapter 2, to gain insight into the difference in therapeutic outcome between gastric and breast cancers, I investigated the treatment induced change in HER2 expression and gene amplification status in gastric cancer using pre- and post-treatment specimens. HER2 is a member of the HER family, which is composed of four transmembrane tyrosine kinase receptors: EGFR, HER2, HER3, and HER4. HER family triggers intracellular signal transduction by activating PI3K/AKT and MAPK pathways, and is involving in regulating cell growth, survival, and apoptosis (Fig. 3) [17]. HER2 is highly expressed in some cancers, such as breast and gastric cancer, resulting in constitutive activation of downstream pathways and contributing to tumor progression and survival (Fig. 3). The phase III Trastuzumab for Gastric Cancer (ToGA) study was the first trial to demonstrate the significant therapeutic benefit of trastuzumab, a humanized monoclonal antibody to HER2, in combination with chemotherapy against HER2-positive gastric or gastro-esophageal junction cancer [18]. The efficacy of continuous

anti-HER2-targeted therapy has been investigated as a second-line treatment. However, both lapatinib and trastuzumab emtansine (T-DM1) failed to prove their clinical benefit [19, 20]. In contrast to gastric cancer, the second-line treatment of using continuous anti-HER2 therapy after the first-line treatment with trastuzumab proved its clinical benefit in breast cancer [21]. One possible cause for this difference can be attributed to the higher intra-tumor heterogeneity of HER2 expression in gastric cancer. In both breast and gastric cancer, it has been reported that previously treated tumors may lose HER2 expression after HER2-targeted therapy [21-25]. The selective pressure of HER2-targeted treatment has been proposed as one of the mechanisms whereby HER2 expression is lost. Previous treatment may preferentially eradicate HER2-overexpressing cells, resulting in the selective survival of HER2-negative tumor cells. In this context, the higher heterogeneity of gastric cancer over breast cancer can facilitate treatment-induced loss of HER2-positive cells. I compared the HER2 expression and gene amplification of paired samples of pre- and post-treated gastric cancers. I found that, in five out of six cases, HER2-positive tumor cells were decreased or lost after treatment. The loss of HER2 can lead to resistance to further anti-HER2 targeted therapy. The high rate of treatment-induced HER2 loss found in gastric cancer is one possible explanation for the disappointing clinical results of second-line anti-HER2 targeted therapy.

Chapter 1: The Balance of Forces Generated by Kinesins Controls Spindle Polarity and Chromosomal Heterogeneity in Tetraploid Cells

Abstract

Chromosomal instability, one of the most prominent features of tumor cells, causes aneuploidy. Tetraploidy is thought to be an intermediate on the path to aneuploidy, but the mechanistic relationship between the two states is poorly understood. Here, I show that spindle polarity (e.g., bipolarity or multipolarity) in tetraploid cells depends on the level of functional phospho-Eg5, a mitotic kinesin, localised at the spindle. Multipolar spindles are formed in cells with high levels of phospho-Eg5. This process is suppressed by inhibition of Eg5 or expression of a non-phosphorylatable Eg5 mutant, as well as by changing the balance between opposing forces required for centrosome separation. Tetraploid cells with high levels of functional Eg5 give rise to a heterogeneous aneuploid population via multipolar division, whereas those with low levels of functional Eg5 continue to undergo bipolar division and remain tetraploid. Furthermore, Eg5 expression levels correlate with ploidy status in tumor specimens. I provide a novel explanation for the tetraploid intermediate model: spindle polarity and subsequent cell behaviour are determined by the balance of forces generated by mitotic kinesins on interpolar microtubules nucleated by supernumerary centrosomes.

Introduction

Aneuploidy, an abnormal number of chromosomes, is a hallmark of cancer and contributes to cancer progression, transformation and drug resistance [3, 22]. Various types of tumor cells show a high rate of chromosome missegregation during cell division, referred to as chromosomal instability (CIN), which results in aneuploid cells [1, 2]. In addition, CIN contributes to tumor heterogeneity, which drives resistance to molecularly targeted therapies [5, 6]. For example, gastric cancer is considered to be highly heterogeneous and it is thus difficult to develop molecularly targeted therapies [7], and approximately half of gastric cancers are categorised as the CIN subtype [2]. Several causes of CIN have been reported, such as spindle assembly checkpoint defects, cohesion defects, hyperstabilised kinetochore-microtubule interactions, centrosome amplification and a tetraploid intermediate [3].

It is believed that aneuploid cells can be generated via the formation of a tetraploid intermediate that has supernumerary centrosomes and a doubled chromosome mass [3, 4, 23, 24]. Tetraploidisation can arise by multiple mechanisms, such as abnormal mitotic exit without chromosome segregation (hereafter referred to as mitotic slippage), cytokinesis failure, p53 activation-dependent mitosis skip, which is observed in senescent cells, and cell fusion [3, 4]. Furthermore, by coupling segregation errors and furrow regression, chromosome nondisjunction mainly results in the generation of tetraploid

cells, rather than directly aneuploid cells with a near-diploid DNA content [12]. Highly aneuploid tumor cells are observed following injection of nude mice with a tetraploid cell fraction, but not with an isogenic diploid cell fraction, generated following treatment with a cytokinesis inhibitor, providing direct evidence of the tetraploid intermediate model [14]. The notion that aneuploid cells accumulate via a tetraploid intermediate is an appealing model to explain the potential importance of the tetraploid status. Indeed, several clinical observations reveal that various premalignant tumors have near-tetraploid DNA contents, such as Barrett's oesophagus and cervical carcinomas [4, 15, 16]. However, it is not fully understood how aneuploid cells are derived from tetraploid cells. The objective of this chapter is to reveal the molecular mechanism of how tetraploid cells generate aneuploidy.

Here, I report that the mitotic kinesin Eg5 (also known as KIF11 or kinesin-5) plays an important role in determining spindle polarity (e.g., multipolarity vs. bipolarity) in tetraploid cells. I demonstrate that spindle multipolarity and subsequent cell behaviour decisions in tetraploid cells are determined by the level of functional Eg5 localised at the spindle, which differs between cell lines. Consequently, Eg5 accelerates the transition of tetraploid cells into heterogenous aneuploid cells.

Materials and Methods

Cell culture, plasmids, RNAi and reagents

HeLa or HCT116 cells were provided by JCRB and ECACC, respectively. HeLa Fucci2 cells were provided by RIKEN BRC through the National Bio-Resource Project of the MEXT, Japan. All cell lines were cultured in DMEM (Gibco) supplemented with 10% foetal bovine serum (FBS), penicillin (100 U/ml) and streptomycin (100 μg/ml). Eg5-specific siRNA (5'-CTGAAGACCTGAAGACAAT-dTdT-3') [25, 26] and luciferase-specific siRNA (GL3; 5'-CUUACGCUGAGUACUUCGAdTdT-3') were synthesised by Sigma. The latter was used as a control. siRNA was transfected using Lipofectamine RNAiMAX (Thermo Fisher). The final concentration of each reagent was as follow: nocodazole (Sigma), 200 ng/ml; paclitaxel (Sigma), 10 μM; monastrol (Calbiochem), 25 μM (HCT116 $p53^{-/-}$) or 100 μM (HeLa); ispinesib (Selleckchem), 10 nM; *S*-trityl-*L*-cysteine (STLC; Sigma), 2 μM; MG132 (Calbiochem), 20 μM; hesperadin (Calbiochem), 50 nM; and thymidine (Sigma), 2.5 mM.

Generation of a HCT116 $p53^{-/-}$ cell line using the CRISPR/Cas9 system

To knockout *TP53* using the CRISPR/Cas9 genome editing system, guide RNA (gRNA) sequences were designed using the online software CRISPRdirect [27]. The targeting sequence of the gRNA was 5'-CTCAGAGGGGGCTCGACGCT-3'. The sense and

antisense oligonucleotides were annealed and cloned into the *Bbs*I site of pX330-U6-Chimeric_BB-CBh-hSpCas9 (Addgene plasmid #42230), which was a gift from Feng Zhang [28]. To construct donor vectors, the DNA fragment was amplified using template DNA (genomic DNA from HCT116 cells), KOD FX DNA polymerase (TOYOBO) and primers (forward: 5'-ACTATATCCTTGTTAACAGGAGGTGGGAGC-3'; and reverse: 5'-AAGGGTGAAGAGGAATCCCAAAGTTCCAAAC-3'), and then cloned into the pCR4-TOPO vector (Thermo Fisher). The amplified and cloned DNA fragment contained two *Bam*HI sites and 600–700 base pairs homologous to the target locus. A puromycin resistance cassette was cloned into the two *BamH*I sites of the amplified and cloned DNA fragments using an In-Fusion HD Cloning Kit (Takara Bio). To establish the HCT116 $p53^{-/-}$ cell line, HCT116 cells were co-transfected with the pX330 plasmid containing the single gRNA target sequence and the donor DNA plasmid using a 4D Nucleofector (Lonza). After puromycin selection, each clone was screened by genomic PCR and sequencing.

Construction and transfection of plasmids

Plasmids encoding full-length $Eg5^{WT}$ and $Eg5^{T926A}$ were gifts from Dr. Wen H. Shen [29]. To generate N-terminally Myc-tagged Eg5-encoding plasmids, PCR was performed using the forward primer 5'-

GTGTCGTGACGCTAGCACCATGGAGCAGAAGCTGATCTCAGAGGAGGACCT GGGATCCGCGTCGCAGCCAAATTCGTC-3' and the reverse primer 5'-GTCCGGTAGCGCTAGTTAAAGGTTGATCTGGGCTCGCAG-3'. The gene encoding Kif15 was PCR-amplified from HeLa cDNA using the forward primer 5'-TACCGAGCTCGGATCCATGGCACCCGGCTGCAAAACTGAG -3' and the reverse primer 5'- CTGGACTAGTGGATCTCAAGATTCACTTCTTTTCTTTTC -3'. The gene encoding HSET was PCR-amplified from HeLa cDNA using the forward primer 5'-GCTAGCCACCATGGATCCGCAGAGGTCCCCCC-3' and the reverse primer 5'-GTCGACTCACTTCCTGTTGGCCTGAGCAG-3'. Myc-Eg5 or HSET was then cloned into the pEF1α-IRES-AcGFP1 vector (631971; Takara Bio) at the *Nhe*I site using an In-Fusion HD Cloning Kit (Takara Bio) or at the *Nhe*I/*Sal*I sites using Ligation high Ver.2 (Toyobo), respectively, according to the manufacturer's instructions. N-terminally 3Myc-tagged Kif15 tagged was cloned into pcDNA3.1 (Thermo Fisher) at the *BsmH*I site using the In-Fusion HD Cloning Kit (Takara Bio). HeLa and HCT116 $p53^{-/-}$ cells were transfected with the plasmids using X-treme GENE 9 (Roche) and X-treme GENE HP (Roche), respectively, according to the manufacturer's instructions.

Immunofluorescence

Cells were grown on collagen-I-coated coverslips (Iwaki) and fixed in pre-cooled

methanol at -20°C (phospho-Eg5/γ-tubulin, Eg5/pericentrin and phospho-Eg5/Myc-tag co-staining) or in 4% paraformaldehyde at 37°C (α-tubulin/pericentrin co-staining) for 15 min. Thereafter, cells were rinsed with phosphate-buffered saline (PBS) containing 10 mM glycine, permeabilised in PBS containing 0.1% Triton X-100 for 5 min, blocked in PBS containing 2% bovine serum albumin (BSA) for 30 min at room temperature and incubated with the following primary antibodies at 4°C: anti-α-tubulin at 1:500 (T6199; Sigma or ab6160; Abcam), anti-pericentrin at 1:500 (ab4448; Abcam), anti-phospho-Eg5 (T926) at 1:5000 (ab61104; Abcam), anti-Eg5 at 1:200 (4203; Cell Signaling), anti-γ-tubulin at 1:2000 (T6557; Sigma) and anti-Myc-tag at 1:8000 (2276; Cell Signaling). Cells were rinsed with PBS, blocked in PBS containing 2% BSA and 2% goat serum and incubated with Alexa Fluor 488-, 568-, 594- and/or 647-conjugated secondary antibodies (Thermo Fisher) diluted 1:2000. Coverslips were washed with PBS containing 4,6-diamidino-2-phenylindole (DAPI) for 5 min, washed with PBS and mounted with Prolong Diamond (Thermo Fisher).

FISH

FISH analyses were performed as previously described [30]. Briefly, cells were grown on collagen-I-coated coverslips (Iwaki) and fixed in Carnoy's fixative solution (methanol:acetic acid, 4:1) at 4°C for 10 min. Coverslips were washed with 2× SSC

buffer and dehydrated in an ethanol series (70%, 85% and 100%; 2 min each following air-drying) that had been pre-cooled to -30°C. DNA probes against the centromeric regions of chromosomes 6 and 18 (Zytovision) conjugated with fluorescent markers (ZyGreen and ZyOrange) were premixed at a ratio of 1:1, warmed to 40°C and placed onto coverslips. Thereafter, coverslips were sealed, denatured at 75°C for 2 min and incubated overnight at 37°C in a humid chamber. Next, coverslips were washed with 4× SSC containing 0.05% Tween 20 for 5 min at room temperature, 0.25× SSC for 2 min at 72°C and 2× SSC containing 0.05% Tween 20 for 30 s at room temperature. Finally, coverslips were incubated with 2× SSC containing HCS CellMask Blue Stain (Invitrogen) at room temperature for 30 min, washed with 2× SSC and mounted using ProLong Diamond (Thermo Fisher) containing DAPI.

Immunohistochemical staining

Tumor specimens from 155 patients with gastric cancer surgically resected between 1995 and 2006 at the Department of Surgery and Science, Kyushu University Hospital, were analysed for Eg5 expression and DNA ploidy. Informed consent was obtained from all patients. The local Ethics Committees of Kyushu University (Study Number 30–148) approved the study. Formalin-fixed, paraffin-embedded cell blocks or tumor specimens were examined for Eg5 expression by immunohistochemistry (IHC). After

deparaffinization, sections were treated with Target Retrieval Solution (pH 6.0; Dako) in a microwave at 95°C for 40 min. After cooling for 30 min at room temperature, the slides were treated with methanol containing 3% H_2O_2 to block endogenous peroxidase activity. After incubation with 10% goat serum for 10 min, the slides were incubated overnight at 4°C with anti-Eg5 antibody diluted 1:100 (4203; Cell Signaling Technology), and then incubated for 1 h with horseradish peroxidase polymer-conjugated secondary antibodies (Dako). Sections were then colour-developed with 3,3'-diaminobenzidine, counterstained with 10% Mayer's hematoxylin, dehydrated, and mounted. Eg5 expression was scored as previously described [31]: 0, no staining or staining in <10% of tumor cells; 1+, weak or detectable staining in ≥10% of tumor cells; 2+, weak to moderate staining in ≥10% of tumor cells; 3+, moderate to strong staining in ≥10% of tumor cells.

Image acquisition and analysis

Immunofluorescence co-staining images were acquired using a Nikon A1R confocal imaging system and an oil immersion Plan-Apo 60× numerical aperture (NA) 1.40 lens (Nikon) or a 100× NA 1.40 lens (Nikon). FISH images were acquired using a Plan-Apo 40× NA 0.95 objective lens (Nikon) on an inverted fluorescence microscope (Nikon Eclipse Ti-E) equipped with a DS-Qi1Mc camera (Nikon). All systems were controlled by Nikon NIS Elements software (Nikon). Maximal-intensity projections were generated

for immunofluorescence co-stained samples. For FISH analyses, Extended depth-of-focus images were generated using the NIS Elements software (Nikon) and acquired images were analysed using IN Cell Developer software (GE Healthcare). Line graphs were generated using NIS Elements software (Nikon). For quantification of the fluorescence of phospho-Eg5, 25 images were acquired as Z-stacks at 0.2 μm intervals and summed. The fluorescence intensities were measured as previously described [30]. For all conditions, I chose a circle that included the whole spindle as the area for quantification. A background circle 1.25-fold larger than the original circle was used to measure the background fluorescence.

Live-cell imaging

HeLa Fucci2 cells were grown in a glass bottom chamber (Matsunami) that had been coated with collagen-I (Nippi) in 5 mM acetic acid at room temperature for 30 min before use. Cells were maintained at 37°C in the presence of 5% CO_2 in a stage-top incubator (Tokai Hit) in the following medium throughout the entire duration of live-cell imaging: FluoroBrite DMEM (Thermo Fisher) supplemented with 10% FBS, penicillin (100 U/ml) and streptomycin (100 μg/ml). Images were acquired every 10 min using a Plan-Apo 20× NA 0.75 lens (Nikon) on an inverted fluorescence microscope (Nikon Eclipse Ti-E) equipped with a DS-Qi2 camera (Nikon).

Flow cytometric analysis of DNA contents

Cells were treated with trypsin, collected, washed with PBS, fixed and stored in 70% ethanol at -30°C for more than 2 h. Thereafter, fixed cells were washed with PBS containing 1% FBS, incubated with PBS containing 1% FBS, 10 μg/ml RNase A and 10 μg/ml propidium iodide at 37°C for 0.5–2 h and analysed using FACSVerse (BD Biosciences). Quantitative analysis was performed using FlowJo software (BD Biosciences)

Analysis of DNA ploidy

Nuclear DNA content was measured by laser-scanning cytometry (LSC; CompuCyte) as described previously [32, 33]. The same paraffin-embedded blocks used for IHC staining were used for this analysis. DNA content histograms were generated and used to determine DNA ploidy. The DNA index (DI) was calculated according to previously published principles [34, 35]. For every case, nuclei were observed after each scan to exclude debris and attached nuclei from the analysis. The DI of G0/G1-phase lymphocytes or fibroblasts was used as a reference, defined as DI = 1.0. Tumors with DI ≤1.2 were defined as diploid; tumors with DI >1.2 and multi-indexed samples were defined as aneuploid.

Cell proliferation assay

Cell proliferation was measured by crystal violet staining. Cells were cultured in 12-well dishes, treated with drugs and fixed in 4% paraformaldehyde at room temperature for 20 min. Thereafter, cells were washed with water, air-dried, stained with 0.05% crystal violet prepared in 20% methanol for 20 min, washed with water and air-dried. Crystal violet were extracted by adding 0.05% NaH_2PO_4 prepared in 50% ethanol and absorbance at 570 nm was measured. The background value was subtracted from all measurements.

Immunoblotting

Cells were harvested and lysed in RIPA buffer (50 mM Tris-HCl pH 8.0, 150 mM NaCl, 0.1% SDS, 1% NP-40, 0.5% deoxycholate, 1 mM PMSF and a protease and phosphatase inhibitor cocktail (Nacalai Tesque)). Mitotic cells were collected by gentle shaking and tapping of the culture vessel (shake-off method). After centrifugation, the supernatants were collected and boiled in SDS loading buffer. Cell lysates were separated by SDS-PAGE and transferred to membranes using the Trans-Blot Turbo Transfer System (Bio-Rad). Immunoblotting was performed using the following primary antibodies at the indicated dilutions: anti-phospho-histone H3 (S10) at 1:1000 (3377; Cell Signaling), anti-Eg5 at 1:2000 (4203; Cell Signaling), anti-phospho-Eg5 (T926) at 1:1000 (ab61104;

Abcam), anti-Myc-tag at 1:1000 (2276; Cell Signaling), anti-KIFC1 at 1:10000 (ab172620; Abcam), anti-Nek2 at 1:1000 (610593; BD Biosciences), and anti-β-actin at 1:5000 (A5316; Sigma). Thereafter, the membranes were incubated with horseradish peroxidase-conjugated secondary antibodies and signals were detected using Chemi-Lumi One (Nacalai Tesque). Quantitative analysis was performed using the ImageJ software [36].

Statistical analyses

Data were analysed using the unpaired two-tailed Student's *t*-test in Figures 4D, 4I, 6C, 6F, 7C, 7F, 8B, 8D, 8F, 8H, and 9B; the Mann-Whitney *U*-test in Figures 4E and 6I; and Fisher's exact test in Figure 9I. Normality of the data and variance between groups were tested. Statistical calculations were carried out using the Prism software (GraphPad).

Results

The effects of Eg5 inhibition are attenuated in tetraploid cells

To prepare tetraploid cells, I synchronised HeLa cells using a thymidine block and release protocol and then treated them with hesperadin, an Aurora B inhibitor, to induce mitotic slippage (Fig. 4A, B) [37, 38]. I studied the mitotic features of tetraploid cells by assessing their responses to anti-mitotic agents. To this end, I treated non-tetraploid and tetraploid HeLa cells with tubulin-binding agents (paclitaxel and nocodazole) or an Eg5 inhibitor (monastrol) and examined their responsiveness. The anti-proliferative effect of monastrol was lower in tetraploid HeLa cells than in non-tetraploid HeLa cells, whereas the efficacies of paclitaxel and nocodazole were similar in these two cell populations (Fig. 4B–D).

Next, I performed live-cell imaging to measure the duration of mitosis in non-tetraploid and tetraploid HeLa cells in the presence of anti-mitotic agents. The duration of mitosis was markedly shorter in tetraploid HeLa cells than in non-tetraploid HeLa cells upon treatment with monastrol, whereas it was slightly shorter in the former cells than in the latter cells upon treatment with paclitaxel or nocodazole (Fig. 4E). In addition, most tetraploid HeLa cells divided in the presence of monastrol, in comparison with only approximately 30% of non-tetraploid HeLa cells (Fig. 4F). By contrast, non-tetraploid and tetraploid HeLa cells responded similarly to paclitaxel and nocodazole (Fig. 4F).

Taken together, I conclude that tetraploid HeLa cells continue to divide upon Eg5 inhibition, resulting in a short duration of mitosis.

Eg5 is a member of the kinesin-5 family of plus-end-directed microtubule-binding motor proteins and is responsible for bipolarisation in mitosis [39-41]. The well-known phenotype induced by monastrol is monopolar spindle formation and mitotic arrest during early mitosis [30, 40, 42]. Mitotic progression continued in most tetraploid HeLa cells upon treatment with monastrol (Fig. 4E–F). To confirm this phenomenon, I treated cells with monastrol and then with MG132, which blocks APC/C-dependent proteolysis, resulting in the accumulation of securin and cyclin B1 and preventing the onset of anaphase. Consistent with previous reports [30, 40, 42], more than 90% of non-tetraploid mitotic HeLa cells were monopolar after treatment with monastrol and MG132. On the other hand, the percentage of bipolar prometaphase cells was significantly higher among tetraploid HeLa cells than among non-tetraploid HeLa cells (Fig. 4G–I). I determined tetraploid status by measuring the number of pericentrin foci (≥3) in mitosis. The results of this analysis strongly suggested that mitotic progression continued in tetraploid cells, but not in non-tetraploid cells, upon monastrol treatment.

Eg5 inhibition suppresses multipolarisation in mitotic tetraploid cells

I further examined mitotic progression in tetraploid HeLa cells upon Eg5 inhibition. A

previous study reported that tetraploid cells, which contain two pairs of centrosomes during mitosis, exhibit multipolar division [43]. Consequently, my finding that the percentage of bipolar prometaphase cells, but not multipolar prometaphase cells, was higher among tetraploid HeLa cells than among non-tetraploid HeLa cells upon Eg5 inhibition (Fig. 4G–I) led me to speculate that Eg5 inhibition might induce bipolar mitosis instead of multipolar mitosis in tetraploid HeLa cells. To test this hypothesis, I determined the mitotic spindle polarities of tetraploid HeLa cells in anaphase and telophase. After tetraploid induction, cells were treated with RO-3306, a CDK1 inhibitor, to inhibit mitotic entry and then released (Fig. 5A). Approximately half of tetraploid HeLa cells underwent multipolar mitosis, resulting in a high rate of chromosome missegregation. On the other hand, almost all monastrol-treated tetraploid HeLa cells underwent bipolar mitosis (Fig. 5B, C). In addition, the missegregation rate was similar in mitotic non-tetraploid HeLa cells and monastrol-treated tetraploid HeLa cells (Fig. 5C). Collectively, I conclude that Eg5 inhibition suppresses multipolar mitosis by promoting bipolar mitosis in tetraploid cells, suggesting that Eg5 plays an essential role in multipolar division of tetraploid HeLa cells.

Spindle pole behaviour is associated with the level of phospho-Eg5 localised at the spindle

Tetraploid HeLa cells exhibited multipolar spindles during mitosis in an Eg5 activity-

dependent manner (Fig. 5). To assess the generality of this phenomenon, I used the HCT116 cell line because it supposedly exhibits chromosomal stability and modal ploidy [44], whereas HeLa cells exhibit CIN and a high level of aneuploidy [45, 46]. Furthermore, because p53 prevents the emergence of tetraploid and aneuploid cells [43, 47, 48], I generated a p53-knockout HCT116 cell line (HCT116 $p53^{-/-}$) using the CRISPR/Cas9 genome editing system. The rate of tetraploid induction was similar in HCT116 $p53^{-/-}$ and HeLa cells after treatment with hesperadin for 12 h (HCT116 $p53^{-/-}$) or 16 h (HeLa). Tetraploid HeLa cells predominantly formed tripolar mitotic spindles, and more than 80% of tetraploid HeLa cells formed multipolar spindles during mitosis (Fig. 6B, C). By contrast, tetraploid HCT116 $p53^{-/-}$ cells predominantly formed bipolar spindles (Fig. 6B, C). I next investigated how these differences between tetraploid HeLa and HCT116 $p53^{-/-}$ cells arose. Eg5 is phosphorylated at an evolutionarily conserved site (T926 in human, T925 in mouse and T937 in *Xenopus*) in its C-terminal bimC box mainly by cyclinB1-CDK1 during mitosis [49, 50]. Phosphorylation of Eg5 at T926 is required for its association with mitotic spindles and thus is essential for the formation of bipolar spindles [49, 51-53]. I examined the expression and phosphorylation (T926) levels of Eg5 in HeLa and HCT116 $p53^{-/-}$ cells. Semi-quantitative analysis revealed that Eg5 expression levels did not markedly differ between HeLa and HCT116 $p53^{-/-}$ cells in mitosis (Fig. 6E). Furthermore, the ratios of phospho-Eg5 to total Eg5 were nearly identical in HeLa and

HCT116 $p53^{-/-}$ cells (Fig. 6F). To further assess the level of phospho-Eg5, I compared the localisation of Eg5 and phospho-Eg5. Phospho-Eg5 clearly localised to the mitotic spindle around the poles during prometaphase and metaphase in HeLa cells, as previously reported (Fig. 6D-H) [29]. The localisation of phospho-Eg5 to these sites was significantly lower in HCT116 $p53^{-/-}$ cells than in HeLa cells (Fig. 6I). Taken together, these data suggest that the level of phospho-Eg5 localised at the spindle correlates with spindle polarity in tetraploid cells.

The level of phospho-Eg5 localised at the spindle affects spindle polarity in tetraploid cells

To confirm the biological significance of phosphorylation-dependent localisation of Eg5 to the spindle for spindle polarity in tetraploid cells, I investigated whether forced changes in the level of phospho-Eg5 altered spindle formation in tetraploid cells. HeLa cells were transfected with plasmids harbouring Myc-tagged wild-type Eg5 (Myc-$Eg5^{WT}$) or a phospho-deficient mutant (Myc-$Eg5^{T926A}$). Overexpression of Myc-$Eg5^{WT}$ led to increased protein levels not only of total Eg5 but also of phosphorylated Eg5 at T926, whereas overexpression of Myc-$Eg5^{T926A}$ only led to an increased protein level of total Eg5 (Fig. 7A). Phospho-Eg5 and Myc-$Eg5^{WT}$ localised to the mitotic spindle in Myc-$Eg5^{WT}$-expressing tetraploid HeLa cells (Fig. 7B). By contrast, Myc-$Eg5^{T926A}$ acted as a dominant-negative protein when highly expressed, and thus decreased the level of

phospho-Eg5 at the mitotic spindle (Fig. 7B; Myc-Eg5^{T926A} upper). The level of phospho-Eg5 at the mitotic spindle was reduced even when expression of Myc-Eg5^{T926A} was low (Fig. 7B; Myc-Eg5^{T926A} middle and lower). Next, I investigated whether reduced localisation of phospho-Eg5 at the mitotic spindle affected spindle polarity in tetraploid HeLa cells. Spindle polarity was similar in mock control and Myc-Eg5^{WT}-overexpressing tetraploid HeLa cells; specifically, most spindles were multipolar. By contrast, the percentages of Myc-Eg5^{T926A}-overexpressing tetraploid HeLa cells with multipolar and bipolar spindles did not significantly differ. In addition, consistent with previous reports [49, 50], the percentage of cells with monopolar spindles was increased among Myc-Eg5^{T926A}-overexpressing tetraploid HeLa cells (Fig. 7C). These data indicate that expression of phospho-deficient Eg5, which disrupted the localisation of phospho-Eg5 to the mitotic spindle, suppressed multipolar spindle formation in tetraploid HeLa cells. Moreover, I examined whether overexpression of Myc-Eg5^{WT} induced the formation of multipolar spindles in tetraploid HCT116 p53$^{-/-}$ cells. Consistent with the observations made in HeLa cells, Myc-Eg5^{WT} was phosphorylated at T926 and localised to the mitotic spindle in HCT116 p53$^{-/-}$ cells (Fig. 7D, E). Overexpression of Myc-Eg5^{WT} significantly increased the percentage of cells with multipolar spindles among tetraploid HCT116 p53$^{-/-}$ cells, but not among diploid HCT116 p53$^{-/-}$ or non-tetraploid HeLa cells (Fig. 7F). This suggests that a high level of phospho-Eg5 induces multipolar spindle formation in

tetraploid cells, but not in diploid cells. Collectively, these results demonstrate that phosphorylation-dependent localisation of Eg5 to the mitotic spindle affects spindle formation in tetraploid cells.

The balance of forces required for centrosome separation affects spindle polarity in tetraploid cells

Multiple kinesins regulate spindle assembly and bipolarisation. Hence, I investigated the involvement of other kinesins in spindle polarity in tetraploid cells. Previous studies revealed that Kif15 (also known as kinesin-12) can coordinate centrosome separation during bipolar spindle assembly when Eg5 activity is inhibited, illustrating the functional flexibility of mitotic kinesins during spindle assembly [25, 54]. To test whether Kif15 cooperates with Eg5 to determine spindle polarization in tetraploid cells, I first investigated the contribution of Kif15 to spindle polarisation in tetraploid HeLa cells using a knockdown/overexpression approach. Knockdown of Kif15 did not change the spindle polarity in tetraploid HeLa cells, indicating that this kinesin does not cooperate with Eg5 to form multipolar spindles in cells with full Eg5 activity (Fig. 8A, B). On the other hand, overexpression of Myc-Kif15 was sufficient to promote multipolar spindles when Eg5 was inhibited by *S*-trityl-*L*-cysteine (STLC), indicating that Kif15 becomes essential for formation of multipolar spindles when Eg5 activity is low or absent (Fig. 8C,

D). Consistent with this, overexpression of Myc-Kif15 significantly increased the proportion of multipolar spindles among tetraploid HCT116 $p53^{-/-}$ cells, which have a low level of functional Eg5 (Fig. 8E, F). Taken together, these data suggest that Kif15 is a potential determinant of spindle polarity, especially in tetraploid cells with low levels of functional Eg5.

Next, I investigated the involvement of a minus-end-directed motor protein in determining spindle polarity in tetraploid cells. HSET (also known as KIFC1 or kinesin-14) is a minus-end-directed motor protein that generates an inward pulling force between spindle poles and regulates microtubule aster formation, centrosome separation and spindle assembly in cooperation with Eg5 [55-57]. The balance between forces generated by Eg5 and HSET is responsible for spindle formation [56, 58]. Therefore, I speculated that changes in HSET expression might alter spindle polarisation in tetraploid HeLa cells, which have multipolar spindles. To investigate this, I examined the phenotype of tetraploid HeLa cells overexpressing HSET. Overexpression of HSET significantly suppressed the formation of multipolar spindles and promoted the formation of bipolar and monopolar spindles in tetraploid HeLa cells (Fig. 8G, H). These results suggest that the balance between opposing forces generated by HSET and Eg5 determine spindle polarisation in tetraploid cells. Collectively, these results demonstrate that spindle polarity (e.g., bipolarisation or multipolarisation) in tetraploid cells is determined by the balance

of forces required for separation of supernumerary centrosomes.

Heterogeneous aneuploid populations are generated from tetraploid cells in an Eg5-dependent manner

To investigate how Eg5-dependent cell division affects subsequent cell behaviours, I examined the DNA contents of tetraploid HeLa and HCT116 $p53^{-/-}$ cells following release from hesperadin and culture for 7 days in the presence or absence of monastrol. The near-diploid population of HeLa cells increased, whereas the tetraploid HCT116 $p53^{-/-}$ cells remained predominantly near-tetraploid (Fig. 9A). Importantly, the percentage of near-diploid cells was significantly higher among tetraploid HeLa cells than among tetraploid HCT116 $p53^{-/-}$ cells after 7 days of culture (Fig. 9B). This is consistent with my observation that multipolar spindles formed more frequently in tetraploid HeLa cells than in tetraploid HCT116 $p53^{-/-}$ cells (Fig. 6). On the other hand, both tetraploid HeLa and HCT116 $p53^{-/-}$ cells remained predominantly near-tetraploid after culture for 7 days in the presence of monastrol (Fig. 9C).

To confirm these observations, I performed fluorescence *in situ* hybridisation (FISH) analysis. After culture in the absence of monastrol, tetraploid HeLa cells contained highly heterogeneous numbers of chromosomes 6 and 18 per cell, and the majority of cells had a chromosome number lower than 4N. By contrast, after culture in the presence of

monastrol, the percentages of cells with 2N or fewer chromosomes were markedly reduced (Fig. 9D, E). On the other hand, the distribution of the number of chromosome foci per cell among aneuploid cells derived from tetraploid HCT116 $p53^{-/-}$ cells was similar in the absence and presence of monastrol (Fig. 9F, G). Taken together, these results strongly suggest that heterogeneous aneuploid populations are generated more efficiently from tetraploid HeLa cells than from tetraploid HCT116 $p53^{-/-}$ cells via changing the distributions of chromosomes in an Eg5 activity-dependent manner.

Finally, I investigated the clinically relevant relationship between Eg5 expression and DNA ploidy in specimens from gastric cancer patients. Consistent with previous studies of Eg5 expression in clinical specimens from breast cancer, hepatocellular carcinoma, and lung cancer [31, 59, 60], I observed a wide range of Eg5 expression levels in gastric cancer specimens (Fig. 9H). I also performed laser-scanning cytometry (LSC) to measure nuclear DNA content in the same paraffin-embedded blocks used for Eg5 IHC staining, and found that a high level of Eg5 expression was associated with DNA aneuploidy in gastric cancer specimens (Fig. 9I). These results indicate that Eg5 overexpression plays a role in the development of aneuploid cells in a clinical context.

Discussion

Tetraploidy is considered to be an intermediate state leading to aneuploidy [14, 24]. Tetraploid cells contain two pairs of centrosomes during mitosis. Consequently, such cells can undergo multipolar mitosis and generate aneuploid progenies [43], and thereby contribute to cancer progression and transformation [4, 14]. In this study, I propose that tetraploid cells are converted into aneuploid cells via multipolar division, which is caused by excessive pushing force generated by Eg5 to separate supernumerary centrosomes (Fig. 10).

Eg5 generates a sliding force to push interpolar microtubules apart, which contributes to bipolarisation. In normal diploid cells, depletion or inhibition of Eg5 results in the formation of monopolar spindles, which leads to prolonged mitotic arrest and apoptosis [42, 61]. However, the same level of Eg5 inhibition does not completely abrogate centrosome separation and spindle polarisation in tetraploid cells; specifically, partial inhibition, resulting in a low level of functional Eg5, suppresses multipolar spindle formation in mitosis. Disruption of the Eg5-dependent interpolar pushing force via overexpression of a non-phosphorylatable Eg5 mutant ($Eg5^{T926A}$) suppressed multipolar spindle formation in tetraploid HeLa cells, which have a high level of functional Eg5. Notably, overexpression of $Eg5^{WT}$ was sufficient to enhance the level of phospho-Eg5, its localisation at the spindle and multipolarisation in tetraploid HCT116 $p53^{-/-}$ cells,

which have a low level of functional Eg5 (Fig. 7). These data strongly suggest that in order to push the supernumerary spindle poles apart, multipolar mitosis in tetraploid cells requires a level of functional Eg5 in excess of that required to promote bipolar spindle formation in non-tetraploid cells.

Tetraploid HeLa cells underwent multipolar mitosis, resulting in the generation of near-diploid cells that were aneuploid and highly heterogeneous, but remained in a near-tetraploid state upon Eg5 inhibition (Fig. 5, 9). Multipolar cell division with a doubled chromosome mass is predicted to cause unequal segregation, leading to gross chromosomal rearrangements and ultimately resulting in cell death due to loss of chromosomes that are essential for survival or proliferation. Consequently, tetraploid cells give rise to aneuploid cells with near-diploid DNA contents upon repeated multipolar divisions. The number of chromosomes in aneuploid cells from cancer patients is predominantly near-diploid and near-tetraploid [4]. Therefore, I speculate that not only aneuploid tumor cells with a near-tetraploid number of chromosomes, but also near-diploid cells can be derived from tetraploid parental cells via multipolar mitosis. HeLa and HCT116 $p53^{-/-}$ cells, in which the level of functional Eg5 localised at the spindle was high and low, respectively, gave rise to different aneuploid populations (Fig. 6, 9). These findings suggest that Eg5 activity at the spindle in parental tumor cells affects the efficiency with which aneuploid cells are generated from tetraploid cells.

Alteration of the level of Eg5 localised at the spindle via overexpression of $Eg5^{WT}$ or a non-phosphorylatable Eg5 mutant affected spindle polarity in tetraploid cells (Fig. 7). Localisation of Myc-$Eg5^{T926A}$ to the spindle was dependent on its expression level (Fig. 7B). Eg5 functions as a homotetramer, which consists of two homodimers arranged in the opposite orientation to each other, to crosslink mitotic spindles and slide microtubules apart [41, 62]. Although the relationship between phosphorylation and tetramerization of Eg5 remains unclear, it is conceivable that Myc-$Eg5^{T926A}$ may be incorporated into the Eg5 tetramer and hence associate with the mitotic spindle when lowly or moderately expressed. By contrast, Myc-$Eg5^{T926A}$ may be assembled into a dominant-negative form of the tetramer that is mainly composed of this mutant when highly expressed, resulting in disruption of its spindle localisation and subsequent monopolar spindle formation. In addition to sliding microtubules apart, Eg5 also functions as a microtubule polymerase that stabilises and increases the growth rate of microtubules [62, 63]. The detailed mechanism by which Eg5 enhances multipolarisation in tetraploid cells remains unclear. In addition to its motor activity, which pushes spindle poles apart, it is conceivable that a higher level of Eg5 might facilitate the separation of proximal supernumerary centrosomes by stabilising interpolar microtubules. Of note, overexpression of Eg5 increased the frequency of multipolar spindle formation in tetraploid cells, but not in diploid cells. This difference might

simply be due to the presence of supernumerary centrosomes and spindles in the former cells. However, the formation of heterogeneous aneuploid populations from tetraploid cells via multipolar division seems to require both supernumerary centrosomes and a doubled chromosome mass. The latter might decrease the probability that essential chromosomes are lost upon multipolar cell division. In fact, the majority of non-tetraploid cells with supernumerary centrosomes die following multipolar division [64, 65].

The activity of Eg5 is regulated in a spatiotemporal manner during mitosis [29, 49, 50, 66]. Consequently, my data do not exclude the possibility that regulators of Eg5 also affect spindle morphology in tetraploid cells. HeLa and HCT116 $p53^{-/-}$ cells contained similar levels of total and phospho-Eg5 (Fig. 6D–G), whereas the level of phospho-Eg5 localised at the spindle clearly differed. This result implies that regulators of the localisation of phospho-Eg5 underlie this difference. PTEN was recently reported to be involved in the regulation of Eg5 and its recruitment to the spindle [29, 66]. Cyclin B1-CDK1 and Nek9-Nek6 phosphorylate Eg5 at T926 and S1003, respectively [49, 67], and protein phosphatase 2A dephosphorylates Eg5 at T926 [68]. By controlling the phosphorylation or recruitment of Eg5 to the spindle, regulators of Eg5 may affect spindle polarity in tetraploid cells. In addition to Eg5, I identified other kinesins responsible for spindle polarity in tetraploid cells: Kif15 and HSET, which are,

respectively, a plus- and a minus-end-directed motor protein. Consistent with previous studies showing that Kif15 is not required for spindle assembly in non-tetraploid HeLa cells with full Eg5 activity [25, 54], multipolar spindle assembly was unaffected by Kif15 knockdown in tetraploid HeLa cells, suggesting that Kif15 is dispensable for determination of spindle polarity in tetraploid cells with high levels of expression or localization of Eg5 at the spindle. On the other hand, in tetraploid cells with a low level of phospho-Eg5, or in which Eg5 is inhibited, Kif15 might act as a key regulator of spindle polarity.

By contrast, overexpression of HSET, which counteracts Eg5 by generating a pulling force between spindle poles, suppressed the formation of multipolar spindles to a similar extent as overexpression of a non-phosphorylatable Eg5 mutant ($Eg5^{T926A}$) (Fig. 7C, 8H). In this context, spindle polarity in tetraploid cells appears to be regulated by multiple factors and the balance between them; however, the interpolar pushing force generated by Eg5 is one of the most important accelerators of multipolar cell division.

In summary, my data provide evidence in support of the tetraploid intermediate model, which describes a possible pathway leading to aneuploidy and tumor heterogeneity. In addition, I report that the balance between opposing forces generated by mitotic kinesins on interpolar microtubules nucleated by supernumerary centrosomes regulates cell behaviour decisions in tetraploid cells. Tetraploid tumor cells with a high

level of functional Eg5 undergo multipolar mitosis, resulting in gross chromosomal rearrangements. On the other hand, tetraploid tumor cells with a low level of functional Eg5 undergo normal-like bipolar mitosis, generating near-tetraploid progenies (Fig. 10). I observed a relationship between high Eg5 expression and DNA aneuploidy in gastric cancer specimens. The existence of a tetraploid population in gastric cancer has been reported previously [69, 70]. Hence, Eg5 overexpression-mediated formation of aneuploidy via a tetraploid intermediate represents one possible pathway to aneuploidy in a clinical context. Furthermore, overexpression of Eg5 has been observed in oral, breast and lung cancers and is associated with a poor prognosis [59, 71, 72]. My data provide a novel possible explanation for these phenomena; a high level of Eg5 can accelerate the acquisition of aneuploidy and chromosomal heterogeneity in tetraploid parental cells, contributing to tumor progression.

Chapter 2: Changes in HER2 Expression and Amplificaction Status Following Preoperative Chemotherapy for Gastric Cancer

Abstract

It is essential to establish a strategy for second-line treatment for human epidermal growth factor receptor 2 (HER2)-positive gastric cancer; however, HER2 expression status after chemotherapy treatment is not routinely determined. I analysed 25 cases of gastric cancer that received preoperative chemotherapy and selected the six pre-treatment samples that were HER2-positive. Pre-and post-treatment tumor samples were examined for HER2 expression, and for *HER2,* epidermal growth factor receptor *(EGFR)*, and hepatocyte growth factor receptor (*HGFR*/*MET)* gene amplification. Three patients had been treated with trastuzumab plus chemotherapy, and three patients with cytotoxic chemotherapy alone. Only one case that had an initial HER2 score of 3+ and had received trastuzumab plus chemotherapy remained HER2-positive after treatment. Decrease or loss of HER2 expression and amplification was observed in the other five patients. Amplification of *EGFR* or *MET* was not observed in any pre-or post-treatment specimens.

My data suggest that trastuzumab plus chemotherapy or chemotherapy alone may induce loss of HER2 positivity.

Introduction

Approximately 10–30% of gastric cancer cases are human epidermal growth factor receptor 2 (HER2)-positive and are possible targets for anti-HER2 therapy [73-77]. The phase III Trastuzumab for Gastric Cancer (ToGA) study was the first trial to demonstrate a significant therapeutic benefit of trastuzumab, a humanized monoclonal antibody to HER2, in combination with chemotherapy against HER2-positive gastric or gastro-esophageal junction cancer [18]. Regarding second-line treatment, the efficacy of continuous anti-HER2-targeted therapy has been investigated. In the TyTAN trial, which explored the efficacy of lapatinib for the second line treatment of HER2-positive advanced gastric cancer, the addition of lapatinib to second-line paclitaxel was not superior compared with placebo plus paclitaxel [19]. In the GATSBY trial, trastuzumab emtansine (T-DM1) was not superior to taxane monotherapy in patients with previously treated HER2-positive gastric or gastro-esophageal junction cancer [20]. It is also noteworthy that in the GATSBY trial, T-DM1 failed to prove its superiority over taxane in patients who had received cytotoxic therapy alone (23%) and in those who had been previously treated with HER2-targeted therapy (77%) [20].

Mechanisms to explain these disappointing results have been proposed. One explanation is that HER2 positivity is lost after HER2-targeted treatment. In breast and gastric cancer, it has been reported that previously treated tumors may lose HER2

expression after HER2-targeted therapy [78-82]. The selective pressure of HER2-targeted treatment has been proposed as one of the mechanisms whereby HER2 expression is lost. Since trastuzumab exerts its antitumor effects against HER2-positive tumor cells [83, 84], it may preferentially eradicate HER2-overexpressing cells, resulting in the selective survival of HER2-negative tumor cells. In addition, gastric cancer has been reported to have greater heterogenicity of HER2 expression than breast cancer [8, 9]. Treatment-induced change in HER2 status may occur more frequently in gastric cancer because HER2-negative tumor cells would become the dominant population in tumors after HER2-targeted therapy. Expression of other receptor tyrosine kinases (RTKs) might be another mechanism that could drive resistance to molecularly targeted therapy through proliferation of non-targeted tumor cells after treatment [85]. Tumors might either initially co-express multiple RTKs or shift their proliferative dependency onto other RTKs following molecularly targeted therapy. Indeed, it has been reported that gastric cancer may co-express HER2, epidermal growth factor receptor (EGFR), and hepatocyte growth factor receptor (HGFR/MET) [86, 87].

Although several mechanisms have been proposed to explain the results of second-line HER2-targeted therapy in gastric cancer, the reason why HER2-targeted therapy has

not shown clinical advantage even in patients not treated with HER2-targeted therapy remains elusive. The objective of this chapter is to reveal the therapy, which is not limited to the HER2-targeted therapy, induced changes in HER2 expression, and provide insight into the influences of heterogeneity on targeted therapy. I focused on patients with gastric cancer who received preoperative chemotherapy and examined the changes in HER2 expression status and amplification of *EGFR* and *MET* not only after HER2-targeted therapy but also after cytotoxic chemotherapy alone.

Materials and Methods

Patients

Twenty-five patients with gastric cancer who received preoperative chemotherapy between 2009 and 2015 at the Department of Surgery and Science, Kyushu University Hospital were analysed. Patients who received neoadjuvant chemotherapy for a resectable tumor and who were converted to surgical resection after chemotherapy were included. Two patients enrolled in a clinical trial were also included in this study. Informed consent was obtained from all patients. The local Ethics Committees of Kyushu University (Study number, 28-68) and Chugai Pharmaceutical Co., Ltd. (Study number, E181) approved the study.

Immunohistochemical staining of HER2

Formalin-fixed, paraffin-embedded pre-and post-treated tumor samples were examined for HER2 expression using immunohistochemistry (IHC). After deparaffinization, sections were treated with Target Retrieval Solution (pH 6.0; Dako, Agilent, Santa Clara, CA, United States) in a microwave at 95°C for 40 min. Slides were then cooled for 30 min at room temperature and treated with methanol containing 3% H_2O_2 to block endogenous peroxidase activity. After incubation with 10% goat serum for 10 min, slides were incubated with an antibody to HER2 (A0485; Dako) at 1:400 dilution overnight at

4°C, and incubated with horseradish peroxidase polymer-conjugated secondary antibodies (Dako) for 1 h. Sections were then color-developed with 3, 3'-diaminobenzidine, counterstained with 10% Mayer's hematoxylin, dehydrated, and mounted. HER2 expression was scored according to previously described scoring criteria [88-90] as follows: Score of 0, no staining or membranous staining in <10% of tumor cells (surgical specimen) or fewer than five cohesive tumor cells (biopsy specimen); score of 1+, weak or detectable staining in only one part of the membrane in ≥10% of tumor cells (surgical specimen) or at least five cohesive tumor cells (biopsy specimen); score of 2+, weak to moderate complete or basolateral membranous staining in ≥10% of tumor cells (surgical specimen) or at least five cohesive tumor cells (biopsy specimen); score of 3+, moderate to strong complete or basolateral membranous staining in ≥10% of tumor cells (surgical specimen) or at least five cohesive tumor cells (biopsy specimen).

Multicolor fluorescence in situ hybridization (FISH) of EGFR, MET, and HER2

Formalin-fixed, paraffin-embedded tumor samples were examined for *HER2, EGFR* and *MET* amplification using FISH. A multicolor FISH probe [EGFR (Cy 5.5)/MET (TexRed)/HER2 (FITC)] was constructed by GSP Laboratory (Kobe, Japan). FISH analysis was performed using pretreatment kit II (GSP Laboratory) according to the manufacturer's instructions. In cases where multicolor FISH signals were faint, samples

were re-analysed using the following dual color FISH probes: *HER2/CEN17, EGFR/CEN7,* and *MET/CEN7* (GSP Laboratory). In all cases, at least 20 cells from more than three different regions of a specimen were examined. *HER2*-amplified cases were defined as those with an average *HER2* gene copy number ≥6 signals per cell or the presence of gene clusters [91]. *EGFR*-or *MET*-amplified cases were defined as these with gene copy number ≥6 signals per cell in ≥40% of cells, ≥15 signals per cell in ≥10% of cells, or the presence of gene clusters in ≥10% of cells [92]. Fluorescence image acquisition was performed using a Nikon A1R confocal imaging system (Nikon Corporation, Tokyo, Japan). The objective lens was an oil immersion Plan-Apo ×60 numerical aperture 1.40 lens (Nikon).

Results

HER2 expression and amplification in patients with gastric cancer who had received preoperative chemotherapy

In 25 patients with gastric cancer who had received preoperative chemotherapy, there were five patients with preoperative biopsy samples that were HER2 3+ and one patient who was HER2 2+ with *HER2* FISH amplification, and thus considered HER2-positive. In order to examine changes in HER2 status after chemotherapy, I assessed the surgical specimens of these six cases of HER2 expression, and also performed FISH for *EGFR/MET/HER2* amplification in pre-and post-treatment specimens (Table 1, 2). As shown in Table 2, all these specimens had *HER2* amplification in the concordant region of the tumor (Fig. 11, 12). Neither *EGFR* nor *MET* were amplified in any of their pre- and post-treatment specimens.

Changes in HER2 expression and amplification after preoperative chemotherapy.

In the six patients who were initially HER2-positive, three patients were treated with trastuzumab in combination with chemotherapy; the other three patients were treated with cytotoxic chemotherapy alone, either S-1, docetaxel, or cisplatin (Table 1). The details of the therapy regimens used are also summarized in Table 1. Patient 1 treated with trastuzumab in combination with chemotherapy had an initial HER2 IHC score of

3+ and HER2 gene amplification. After treatment, HER2 expression and amplification were retained in the surgical specimen from the same patient (Table 2, Fig. 11). In the post-treatment specimen of this case, HER2-positive tumor cells were observed in the mid-portion of the tissue and HER2-negative tumor cells were seen in the epithelial portion (Fig. 11). Two other patients who had received trastuzumab in combination with chemotherapy showed a decrease or loss of HER2 expression and amplification in post-treatment surgical specimens (patients 2 and 3 in Table 2). We also found that in all three cases treated with cytotoxic chemotherapy alone, HER2 expression was lost (IHC score 0) after treatment (Fig. 12, patients 4–6 in Table 2). In their post-treatment specimens, loss of *HER2* gene amplification was also confirmed in all three cases using FISH. Results are summarized in Table 2.

Discussion

Since trastuzumab demonstrated a significant overall survival advantage as first-line therapy for advanced HER2-positive gastric cancer [18], the HER2 signaling pathway is considered to be a driver pathway of proliferation in HER2-positive gastric tumor cells. Although HER2-targeted therapy has been commonly used in second-line treatment of HER2-positive breast cancer [93], it has failed to be established as second-line treatment in gastric cancer. Consistent with previous studies in gastric cancer [80-82], I found that two out of three patients with HER2-positive disease treated with trastuzumab in combination with chemotherapy were converted to HER2-negative. In addition, my data suggest that cytotoxic chemotherapy can also lead to loss of HER2-positive tumor cells. The loss of HER2 was confirmed by both protein expression and gene amplification analyses, suggesting that the loss of HER2 expression observed was not due to inappropriate IHC staining conditions that would affect IHC scores [94].

In breast cancer, Guarneri *et al.* reported that HER2 loss was observed more frequently after cytotoxic chemotherapy alone than after chemotherapy in combination with anti-HER2 targeted therapy (40% *versus* 14.7%) [78]. Although the reason for this phenomenon observed in the current study and in the breast cancer study is unclear, several preclinical studies showed that HER2 overexpression would promote proliferation of tumor cells [95, 96]. Therefore, one possible explanation for cytotoxic

chemotherapy-induced loss of HER2 is that HER2-positive gastric cancer cells may proliferate faster than other tumor cells therefore they would be more sensitive to cytotoxic therapies. Indeed, several clinical studies support the hypothesis that HER2-positive tumors are more sensitive to chemotherapy [97, 98], suggesting that, like HER2-targeted therapy, cytotoxic therapy may also preferentially eliminate HER2-positive clones, resulting in loss of HER2 positivity. This finding may provide a possible explanation for the result of the GATSBY trial, in which T-DM1 did not show superior clinical benefit compared with taxane in patients who were previously treated with or without HER2-targeted therapy.

Because it has been shown that molecular heterogeneity and receptor co-amplification can drive resistance to targeted therapies [85], I investigated whether the tumors had co-amplification of *EGFR* or *MET* and whether amplification would be affected by chemotherapy. In my data, neither *EGFR* nor *MET* were amplified in pre-and post-treatment specimens, suggesting that *EGFR*- or *MET*-amplified tumor cells did not pre-exist or arise during chemotherapy treatment in these cases. However, I cannot rule out the involvement of other RTKs or downstream signaling factors that were previously reported to be amplified or overexpressed in gastric cancer [99, 100].

My work has some limitations. Firstly, since my results are based on a small sample size, it is difficult to estimate the rate of change of HER2 expression after chemotherapy

statistically. Secondly, discordance of HER2 expression between biopsy and surgical specimens may also have influenced the results [101, 102]. Biopsy specimens may fail to reflect HER2 expression in the whole tumor. Thus, there is still the possibility that I overestimated HER2 expression in pre-treatment specimens. Therefore, further comprehensive assessments are warranted.

In conclusion, I assessed HER2 status after preoperative chemotherapy and found that cytotoxic chemotherapy alone could lead to loss of HER2 expression and gene amplification. My data suggest that even in cases that have not previously received HER2-targeted therapy, it is critically important to reassess HER2 expression prior to treatment with HER2-targeted therapy. In order to accurately evaluate efficacy of second-line HER2-targeted therapy in gastric cancer, future clinical trials need to be designed such that only patients who remain HER2-positive after previous chemotherapy treatment are eligible.

General Discussion

Since the CIN and aneuploidy are the most prominent features of tumors, I investigated the process leading to aneuploidy and its influence on treatment outcome. In chapter 1, I propose that the balance of forces between mitotic spindles generated by mitotic kinesins, such as Eg5, determines the spindle polarity in tetraploid cells (Fig. 10). An imbalance between pushing- or pulling-force will affect the subsequent population of progenies. Pushing-force dominant tetraploid cells preferentially undergo multipolar divisions, leading to heterogeneous aneuploidy. In chapter 2, I compared paired pre- and post-treated tumor specimens of gastric cancer to gain insight into mechanisms of resistance to second-line targeted therapy. I found that HER2 expressions and gene amplifications can be lost after anti-tumor therapies, which are not limited to anti-HER2 targeted therapy (Fig. 13). Consequently, the loss of tumor cells that express the molecular target would result in resistance to the subsequent targeted therapy.

In chapter 1, in assessing cells and tumor specimens, I found that Eg5 expression varies considerably among tumor cells. In this situation, once spontaneously tetraploid cells are derived, they can be easily transformed to aneuploid population if they overexpress Eg5. The frequency and the leading cause of the emergence of tetraploid tumor cells in clinical contexts are unclear. It is difficult to estimate how frequently tetraploid cells appear during tumorigenesis because tetraploid cells are intermediates; this is supposedly a short-

lived state. However, analysing the number of chromosomes in cancer cells suggests that specific cancer types would more potently generate tetraploid cells. Although diploid or near-diploid cells dominate in most cancer types, several cancers—prostate, liver, and cervix cancer—have a relatively high proportion of near-tetraploid chromosome numbers (Fig. 1) [4]. In addition, through repeated multipolar division, tetraploid cells can give rise to aneuploid cells with substantially reduced chromosome numbers. Accordingly, estimating frequency simply by measuring the distribution of chromosome numbers in cancers may underestimate the frequency of tetraploid intermediates.

I have shown that Eg5 determines polarization in tetraploid cells. In normal diploid cells, Eg5 is essential for bipolarisation during the mitotic process. The depletion or inhibition of Eg5 results in the formation of monopolar spindles, which leads to prolonged mitotic arrest and apoptosis [42, 61]. In addition, Eg5 specific inhibitors show strong efficacy in preclinical cancer xenograft models [103]. Therefore, more than 38 clinical trials involving Eg5-targeting agents have been conducted [39]. Yet despite promising preclinical results, Eg5-targeting agents have only had a moderate effect in the clinical context. Some hypotheses have been proposed to explain the clinical results. One hypothesis is that the doubling times in human tumors (> 100 days) are much longer than those in xenograft models (several days) [104]. This means that only a small percentage of tumor cells are undergoing mitosis when Eg5-targeting agents are administrated.

Another potential reason is the ability of Kif15 to substitute for Eg5. A previous study showed that Kif15 can assume the essential role of Eg5 in bipolar spindle formation when Eg5 was inactivated by an inhibitor. Therefore, Kif15 is supposedly one of the resistant mechanisms for Eg5-targeting agents [25, 54]. Tetraploid tumor cells are another explanation for the poor efficacy of Eg5-targeting agents. As I have shown, because tetraploid cells can continue mitosis in the presence of the Eg5 inhibitor, they are more resistant to Eg5 inhibition than diploid cells (Fig. 4C-H).

To summarize chapter 1, I observed a relationship between high Eg5 expression and DNA aneuploidy in gastric cancer specimens. Further investigation of Eg5 expression and aneuploidy in various cancers would provide insight into how aneuploidy is acquired.

In chapter 2, by examining the changes in HER2 expression and gene expression in gastric cancer specimens, I indirectly assessed the influence of heterogeneity on acquired drug resistance. Breast and gastric cancer share HER2 as a common molecule that can be targeted by anti-HER2 agents. However, the responses to second-line anti-HER2 therapy is different; breast cancer still responds to continuous anti-HER2 treatment, but gastric cancer does not. Gastric cancer is considered to be a highly heterogeneous cancer [7]. I hypothesized that the heterogeneous expression of HER2 in gastric cancer is a resistant mechanism to the continuous anti-HER2 therapy. I observed heterogeneous intra-tumor

HER2 expression patterns (Fig. 11, 12). The HER2 protein expression and gene amplification were concordant in the tumor regions I examined, suggesting that gene amplification resulted in HER2 overexpression. In 5 out of 6 post-treated specimens, both HER2 overexpressed and amplified cells were lost. This means that the treatment eliminated HER2-positive cells directly rather than regulating protein expression. This result also suggests that heterogeneity can accelerate the resistance to molecular targeted therapy by inducing loss of the target (Fig. 13). However, sampled biopsy specimens sometimes fail to reflect whole tumors. Therefore, to elucidate a more accurate relationship between heterogeneity and the loss of target molecules during treatment, a comprehensive analysis of the heterogeneity of pre-treated biopsy specimens is needed in a future study. Furthermore, I unexpectedly found that not only anti-HER2 therapy, but also chemotherapy can induce loss of HER2. This warrants the further examination of the rate of HER2 expression conversion after various therapies. In the current clinical context, the risk of heterogeneity in cancer cells is not sufficiently considered. In most cases, HER2 expression is assessed only once before starting first-line treatment. My results suggest that it is critically important to reassess HER2 expression before making a decision about second-line treatment, especially with highly heterogeneous cancers.

In summary, CIN drives cancer to heterogeneity through several mechanisms,

including tetraploid intermediates. I propose that Eg5 promotes heterogeneity by accelerating multipolar division in tetraploid cells. Thereafter, heterogeneous tumors can acquire resistance to targeted therapies by inducing the loss of target molecules such as HER2. Heterogeneity in cancer should be taken into consideration when making decisions about treatment. Further investigations into common fragility in CIN are needed to target heterogeneous cancers.

Acknowledgements

I am deeply grateful to Associate Professor Hidekazu Kuwayama, Professor Kenji Miura, Professor Kentaro Nakano, and Associate Professor Kazuichi Sakamoto, University of Tsukuba, for guidance and valuable discussion through my doctoral program.

I express my special thanks to Associate Professor Makoto Iimori, Kyushu University, for guiding, supporting and discussing my work.

I appreciate Mr. Takeshi Wakasa, Taiho Pharmaceutical Co. Ltd., for his contributions.

I appreciate Dr. Eiji Oki, Dr. Koji Ando, Dr. Tomoko Jogo, Dr. Ryota Nakanishi, Professor Hiroshi Saeki, Professor Yoshinao Oda, and Professor Yoshihiko Maehara, Kyushu University, for their helpful and valuable suggestions and supports.

I thank Professor Hiroyuki Kitao, Kyushu University, and Mr. Yuki Kataoka, Taiho Pharmaceutical Co. Ltd., for their helpful and valuable discussion.

I also thank Yuko Kubota, Atsuko Yamaguchi, Masako Kosugi, Naoko Katakura, Kyushu University, for their professional technical support.

Finally, I would like to appreciate my family for supporting my life in University of Tsukuba.

References

1. Hanahan, D. and R.A. Weinberg, *Hallmarks of cancer: the next generation.* Cell, 2011. **144**(5): p. 646-74.
2. Cancer Genome Atlas Research, N., *Comprehensive molecular characterization of gastric adenocarcinoma.* Nature, 2014. **513**(7517): p. 202-9.
3. Storchova, Z. and D. Pellman, *From polyploidy to aneuploidy, genome instability and cancer.* Nat Rev Mol Cell Biol, 2004. **5**(1): p. 45-54.
4. Storchova, Z. and C. Kuffer, *The consequences of tetraploidy and aneuploidy.* J Cell Sci, 2008. **121**(Pt 23): p. 3859-66.
5. Fisher, R., L. Pusztai, and C. Swanton, *Cancer heterogeneity: implications for targeted therapeutics.* British Journal Of Cancer, 2013. **108**: p. 479.
6. Heng, H.H., et al., *Chromosomal instability (CIN): what it is and why it is crucial to cancer evolution.* Cancer Metastasis Rev, 2013. **32**(3-4): p. 325-40.
7. Alsina, M., I. Gullo, and F. Carneiro, *Intratumoral heterogeneity in gastric cancer: a new challenge to face.* Ann Oncol, 2017. **28**(5): p. 912-913.
8. Lee, H.E., et al., *Clinical significance of intratumoral HER2 heterogeneity in gastric cancer.* Eur J Cancer, 2013. **49**(6): p. 1448-57.
9. Yang, J., et al., *Intratumoral heterogeneity determines discordant results of diagnostic tests for human epidermal growth factor receptor (HER) 2 in gastric cancer specimens.* Cell Biochem Biophys, 2012. **62**(1): p. 221-8.
10. Duelli, D.M., et al., *A primate virus generates transformed human cells by fusion.* The Journal of Cell Biology, 2005. **171**(3): p. 493-503.
11. Brito, D.A. and C.L. Rieder, *Mitotic checkpoint slippage in humans occurs via cyclin B destruction in the presence of an active checkpoint.* Curr Biol, 2006. **16**(12): p. 1194-200.
12. Shi, Q. and R.W. King, *Chromosome nondisjunction yields tetraploid rather than aneuploid cells in human cell lines.* Nature, 2005. **437**(7061): p. 1038-42.
13. Daniels, M.J., et al., *Abnormal cytokinesis in cells deficient in the breast cancer susceptibility protein BRCA2.* Science, 2004. **306**(5697): p. 876-9.
14. Fujiwara, T., et al., *Cytokinesis failure generating tetraploids promotes tumorigenesis in p53-null cells.* Nature, 2005. **437**(7061): p. 1043-7.
15. Galipeau, P.C., et al., *17p (p53) allelic losses, 4N (G2/tetraploid) populations, and progression to aneuploidy in Barrett's esophagus.* Proc Natl Acad Sci U S A, 1996. **93**(14): p. 7081-4.
16. Olaharski, A.J., et al., *Tetraploidy and chromosomal instability are early events during cervical carcinogenesis.* Carcinogenesis, 2006. **27**(2): p. 337-43.
17. Arteaga, C.L., et al., *Treatment of HER2-positive breast cancer: current status*

and future perspectives. Nature Reviews Clinical Oncology, 2012. **9**(1): p. 16-32.
18. Bang, Y.J., et al., *Trastuzumab in combination with chemotherapy versus chemotherapy alone for treatment of HER2-positive advanced gastric or gastro-oesophageal junction cancer (ToGA): a phase 3, open-label, randomised controlled trial.* Lancet, 2010. **376**(9742): p. 687-97.
19. Satoh, T., et al., *Lapatinib plus paclitaxel versus paclitaxel alone in the second-line treatment of HER2-amplified advanced gastric cancer in Asian populations: TyTAN--a randomized, phase III study.* J Clin Oncol, 2014. **32**(19): p. 2039-49.
20. Thuss-Patience, P.C., et al., *Trastuzumab emtansine versus taxane use for previously treated HER2-positive locally advanced or metastatic gastric or gastro-oesophageal junction adenocarcinoma (GATSBY): an international randomised, open-label, adaptive, phase 2/3 study.* Lancet Oncol, 2017. **18**(5): p. 640-653.
21. Verma, S., et al., *Trastuzumab emtansine for HER2-positive advanced breast cancer.* New England Journal of Medicine, 2012. **367**(19): p. 1783-1791.
22. Holland, A.J. and D.W. Cleveland, *Losing balance: the origin and impact of aneuploidy in cancer.* EMBO Rep, 2012. **13**(6): p. 501-14.
23. King, R.W., *When 2+2=5: the origins and fates of aneuploid and tetraploid cells.* Biochim Biophys Acta, 2008. **1786**(1): p. 4-14.
24. Ganem, N.J., Z. Storchova, and D. Pellman, *Tetraploidy, aneuploidy and cancer.* Curr Opin Genet Dev, 2007. **17**(2): p. 157-62.
25. Sturgill, E.G., et al., *Kinesin-5 inhibitor resistance is driven by kinesin-12.* J Cell Biol, 2016. **213**(2): p. 213-27.
26. Weil, D., et al., *Targeting the kinesin Eg5 to monitor siRNA transfection in mammalian cells.* Biotechniques, 2002. **33**(6): p. 1244-8.
27. Naito, Y., et al., *CRISPRdirect: software for designing CRISPR/Cas guide RNA with reduced off-target sites.* Bioinformatics, 2015. **31**(7): p. 1120-3.
28. Cong, L., et al., *Multiplex genome engineering using CRISPR/Cas systems.* Science, 2013. **339**(6121): p. 819-23.
29. He, J., et al., *PTEN regulates EG5 to control spindle architecture and chromosome congression during mitosis.* Nat Commun, 2016. **7**: p. 12355.
30. Iimori, M., et al., *Phosphorylation of EB2 by Aurora B and CDK1 ensures mitotic progression and genome stability.* Nat Commun, 2016. **7**: p. 11117.
31. Saijo, T., et al., *Eg5 expression is closely correlated with the response of advanced non-small cell lung cancer to antimitotic agents combined with platinum chemotherapy.* Lung Cancer, 2006. **54**(2): p. 217-25.

32. Otsu, H., et al., *Gastric Cancer Patients with High PLK1 Expression and DNA Aneuploidy Correlate with Poor Prognosis.* Oncology, 2016. **91**(1): p. 31-40.
33. Ando, K., et al., *High expression of BUBR1 is one of the factors for inducing DNA aneuploidy and progression in gastric cancer.* Cancer Sci, 2010. **101**(3): p. 639-45.
34. Furuya, T., et al., *Relationship between chromosomal instability and intratumoral regional DNA ploidy heterogeneity in primary gastric cancers.* Clin Cancer Res, 2000. **6**(7): p. 2815-20.
35. Hiddemann, W., et al., *Convention on nomenclature for DNA cytometry. Committee on Nomenclature, Society for Analytical Cytology.* Cancer Genet Cytogenet, 1984. **13**(2): p. 181-3.
36. Schneider, C.A., W.S. Rasband, and K.W. Eliceiri, *NIH Image to ImageJ: 25 years of image analysis.* Nat Methods, 2012. **9**(7): p. 671-5.
37. Tsuda, Y., et al., *Mitotic slippage and the subsequent cell fates after inhibition of Aurora B during tubulin-binding agent-induced mitotic arrest.* Sci Rep, 2017. **7**(1): p. 16762.
38. Hauf, S., et al., *The small molecule Hesperadin reveals a role for Aurora B in correcting kinetochore-microtubule attachment and in maintaining the spindle assembly checkpoint.* J Cell Biol, 2003. **161**(2): p. 281-94.
39. Rath, O. and F. Kozielski, *Kinesins and cancer.* Nat Rev Cancer, 2012. **12**(8): p. 527-39.
40. Kapoor, T.M., et al., *Probing spindle assembly mechanisms with monastrol, a small molecule inhibitor of the mitotic kinesin, Eg5.* J Cell Biol, 2000. **150**(5): p. 975-88.
41. Sawin, K.E., et al., *Mitotic spindle organization by a plus-end-directed microtubule motor.* Nature, 1992. **359**(6395): p. 540-3.
42. Mayer, T.U., et al., *Small molecule inhibitor of mitotic spindle bipolarity identified in a phenotype-based screen.* Science, 1999. **286**(5441): p. 971-4.
43. Vitale, I., et al., *Multipolar mitosis of tetraploid cells: inhibition by p53 and dependency on Mos.* EMBO J, 2010. **29**(7): p. 1272-84.
44. Roschke, A.V., et al., *Stable Karyotypes in Epithelial Cancer Cell Lines Despite High Rates of Ongoing Structural and Numerical Chromosomal Instability.* Neoplasia (New York, N.Y.), 2002. **4**(1): p. 19-31.
45. Landry, J.J., et al., *The genomic and transcriptomic landscape of a HeLa cell line.* G3 (Bethesda), 2013. **3**(8): p. 1213-24.
46. Macville, M., et al., *Comprehensive and definitive molecular cytogenetic*

characterization of HeLa cells by spectral karyotyping. Cancer Res, 1999. **59**(1): p. 141-50.

47. Castedo, M., et al., *Apoptosis regulation in tetraploid cancer cells.* EMBO J, 2006. **25**(11): p. 2584-95.
48. Thompson, S.L. and D.A. Compton, *Proliferation of aneuploid human cells is limited by a p53-dependent mechanism.* J Cell Biol, 2010. **188**(3): p. 369-81.
49. Blangy, A., et al., *Phosphorylation by p34cdc2 regulates spindle association of human Eg5, a kinesin-related motor essential for bipolar spindle formation in vivo.* Cell, 1995. **83**(7): p. 1159-69.
50. Cahu, J., et al., *Phosphorylation by Cdk1 Increases the Binding of Eg5 to Microtubules In Vitro and in Xenopus Egg Extract Spindles.* PLoS ONE, 2008. **3**(12): p. e3936.
51. Chee, M.K. and S.B. Haase, *B-cyclin/CDKs regulate mitotic spindle assembly by phosphorylating kinesins-5 in budding yeast.* PLoS Genet, 2010. **6**(5): p. e1000935.
52. Sawin, K.E. and T.J. Mitchison, *Mutations in the kinesin-like protein Eg5 disrupting localization to the mitotic spindle.* Proc Natl Acad Sci U S A, 1995. **92**(10): p. 4289-93.
53. Avunie-Masala, R., et al., *Phospho-regulation of kinesin-5 during anaphase spindle elongation.* J Cell Sci, 2011. **124**(Pt 6): p. 873-8.
54. Tanenbaum, M.E., et al., *Kif15 cooperates with eg5 to promote bipolar spindle assembly.* Curr Biol, 2009. **19**(20): p. 1703-11.
55. She, Z.-Y. and W.-X. Yang, *Molecular mechanisms of kinesin-14 motors in spindle assembly and chromosome segregation.* Journal of Cell Science, 2017. **130**(13): p. 2097-2110.
56. Mountain, V., et al., *The kinesin-related protein, HSET, opposes the activity of Eg5 and cross-links microtubules in the mammalian mitotic spindle.* J Cell Biol, 1999. **147**(2): p. 351-66.
57. Norris, S.R., et al., *Microtubule minus-end aster organization is driven by processive HSET-tubulin clusters.* Nat Commun, 2018. **9**(1): p. 2659.
58. Kim, N. and K. Song, *KIFC1 is essential for bipolar spindle formation and genomic stability in the primary human fibroblast IMR-90 cell.* Cell Struct Funct, 2013. **38**(1): p. 21-30.
59. Jin, Q., et al., *High Eg5 expression predicts poor prognosis in breast cancer.* Oncotarget, 2017. **8**(37): p. 62208-62216.
60. Liu, C., et al., *Eg5 Overexpression Is Predictive of Poor Prognosis in*

Hepatocellular Carcinoma Patients. Dis Markers, 2017. **2017**: p. 2176460.

61. Tao, W., et al., *Induction of apoptosis by an inhibitor of the mitotic kinesin KSP requires both activation of the spindle assembly checkpoint and mitotic slippage.* Cancer Cell, 2005. **8**(1): p. 49-59.
62. Kapitein, L.C., et al., *The bipolar mitotic kinesin Eg5 moves on both microtubules that it crosslinks.* Nature, 2005. **435**(7038): p. 114-8.
63. Chen, Y. and W.O. Hancock, *Kinesin-5 is a microtubule polymerase.* Nat Commun, 2015. **6**: p. 8160.
64. Sercin, O., et al., *Transient PLK4 overexpression accelerates tumorigenesis in p53-deficient epidermis.* Nat Cell Biol, 2016. **18**(1): p. 100-10.
65. Ganem, N.J., S.A. Godinho, and D. Pellman, *A mechanism linking extra centrosomes to chromosomal instability.* Nature, 2009. **460**(7252): p. 278-82.
66. van Ree, J.H., et al., *Pten regulates spindle pole movement through Dlg1-mediated recruitment of Eg5 to centrosomes.* Nat Cell Biol, 2016. **18**(7): p. 814-21.
67. Rapley, J., et al., *The NIMA-family kinase Nek6 phosphorylates the kinesin Eg5 at a novel site necessary for mitotic spindle formation.* J Cell Sci, 2008. **121**(Pt 23): p. 3912-21.
68. Liu, Y., et al., *Protein Phosphatase 2A (PP2A) Regulates EG5 to Control Mitotic Progression.* Sci Rep, 2017. **7**(1): p. 1630.
69. Abarbanel, J., et al., *Cytogenetic studies in patients with gastric cancer.* World J Surg, 1991. **15**(6): p. 778-82.
70. Tsushima, K., et al., *Correlation of DNA ploidy, histopathology, stage and clinical outcome in gastric carcinoma.* Surg Oncol, 1992. **1**(1): p. 17-25.
71. Daigo, K., et al., *Characterization of KIF11 as a novel prognostic biomarker and therapeutic target for oral cancer*. 2017.
72. Kato, T., et al., *Personalized siRNA-Nanoparticle Systemic Therapy using Metastatic Lymph Node Specimens Obtained with EBUS-TBNA in Lung Cancer.* Molecular Cancer Research, 2018. **16**(1): p. 47.
73. Cutsem, E.V., et al., *Efficacy results from the ToGA trial: A phase III study of trastuzumab added to standard chemotherapy (CT) in first-line human epidermal growth factor receptor 2 (HER2)-positive advanced gastric cancer (GC).* Journal of Clinical Oncology, 2009. **27**(18S): p. LBA4509-LBA4509.
74. Gravalos, C. and A. Jimeno, *HER2 in gastric cancer: a new prognostic factor and a novel therapeutic target.* Ann Oncol, 2008. **19**(9): p. 1523-9.
75. He, C., et al., *Correlation of human epidermal growth factor receptor 2 expression with clinicopathological characteristics and prognosis in gastric cancer.* World J

Gastroenterol, 2013. **19**(14): p. 2171-8.
76. Kim, K.C., et al., *Evaluation of HER2 protein expression in gastric carcinomas: comparative analysis of 1,414 cases of whole-tissue sections and 595 cases of tissue microarrays.* Ann Surg Oncol, 2011. **18**(10): p. 2833-40.
77. Otsu, H., et al., *Correlation of HER2 expression with clinicopathological characteristics and prognosis in resectable gastric cancer.* Anticancer Res, 2015. **35**(4): p. 2441-6.
78. Guarneri, V., et al., *Loss of HER2 positivity and prognosis after neoadjuvant therapy in HER2-positive breast cancer patients.* Ann Oncol, 2013. **24**(12): p. 2990-4.
79. Mittendorf, E.A., et al., *Loss of HER2 amplification following trastuzumab-based neoadjuvant systemic therapy and survival outcomes.* Clin Cancer Res, 2009. **15**(23): p. 7381-8.
80. Ishimine, Y., et al., *Loss of HER2 Positivity after Trastuzumab in HER2-Positive Gastric Cancer: Is Change in HER2 Status Significantly Frequent?* Case Reports in Gastrointestinal Medicine, 2015. **2015**: p. 132030.
81. Pietrantonio, F., et al., *HER2 loss in HER2-positive gastric or gastroesophageal cancer after trastuzumab therapy: Implication for further clinical research.* Int J Cancer, 2016. **139**(12): p. 2859-2864.
82. Seo, S., et al., *Loss of HER2 positivity after anti-HER2 chemotherapy in HER2-positive gastric cancer patients: Results of GASTric cancer HER2 reassessment study 3 (GASTHER3).* Journal of Clinical Oncology, 2017. **35**(4_suppl): p. 27-27.
83. Baselga, J., et al., *Recombinant humanized anti-HER2 antibody (Herceptin) enhances the antitumor activity of paclitaxel and doxorubicin against HER2/neu overexpressing human breast cancer xenografts.* Cancer Res, 1998. **58**(13): p. 2825-31.
84. Fujimoto-Ouchi, K., et al., *Antitumor activity of trastuzumab in combination with chemotherapy in human gastric cancer xenograft models.* Cancer Chemother Pharmacol, 2007. **59**(6): p. 795-805.
85. Kwak, E.L., et al., *Molecular Heterogeneity and Receptor Coamplification Drive Resistance to Targeted Therapy in MET-Amplified Esophagogastric Cancer.* Cancer Discov, 2015. **5**(12): p. 1271-81.
86. Fuse, N., et al., *Prognostic impact of HER2, EGFR, and c-MET status on overall survival of advanced gastric cancer patients.* Gastric Cancer, 2016. **19**(1): p. 183-91.
87. Nagatsuma, A.K., et al., *Expression profiles of HER2, EGFR, MET and FGFR2*

in a large cohort of patients with gastric adenocarcinoma. Gastric Cancer, 2015. **18**(2): p. 227-38.

88. Abrahao-Machado, L.F. and C. Scapulatempo-Neto, *HER2 testing in gastric cancer: An update.* World J Gastroenterol, 2016. **22**(19): p. 4619-25.
89. Hofmann, M., et al., *Assessment of a HER2 scoring system for gastric cancer: results from a validation study.* Histopathology, 2008. **52**(7): p. 797-805.
90. Ruschoff, J., et al., *HER2 diagnostics in gastric cancer-guideline validation and development of standardized immunohistochemical testing.* Virchows Arch, 2010. **457**(3): p. 299-307.
91. Hanna, W.M., et al., *HER2 in situ hybridization in breast cancer: clinical implications of polysomy 17 and genetic heterogeneity.* Mod Pathol, 2014. **27**(1): p. 4-18.
92. Varella-Garcia, M., et al., *EGFR fluorescence in situ hybridisation assay: guidelines for application to non-small-cell lung cancer.* J Clin Pathol, 2009. **62**(11): p. 970-7.
93. Verma, S., et al., *Trastuzumab emtansine for HER2-positive advanced breast cancer.* N Engl J Med, 2012. **367**(19): p. 1783-91.
94. Yamashita-Kashima, Y., et al., *Importance of formalin fixing conditions for HER2 testing in gastric cancer: immunohistochemical staining and fluorescence in situ hybridization.* Gastric Cancer, 2014. **17**(4): p. 638-647.
95. Chi, F., et al., *HER2 induces cell proliferation and invasion of non-small-cell lung cancer by upregulating COX-2 expression via MEK/ERK signaling pathway.* Onco Targets Ther, 2016. **9**: p. 2709-16.
96. Eladdadi, A. and D. Isaacson, *A mathematical model for the effects of HER2 overexpression on cell proliferation in breast cancer.* Bull Math Biol, 2008. **70**(6): p. 1707-29.
97. Baselga, J., et al., *HER2 overexpression and paclitaxel sensitivity in breast cancer: therapeutic implications.* Oncology (Williston Park), 1997. **11**(3 Suppl 2): p. 43-8.
98. Muss, H.B., et al., *c-erbB-2 expression and response to adjuvant therapy in women with node-positive early breast cancer.* N Engl J Med, 1994. **330**(18): p. 1260-6.
99. Jia, Y.-X., et al., *The coexpression and prognostic significance of c-MET, fibroblast growth factor receptor 2, and human epidermal growth factor receptor 2 in resected gastric cancer: a retrospective study.* OncoTargets and therapy, 2016. **9**: p. 5919-5929.

100. Stahl, P., et al., *Heterogeneity of amplification of HER2, EGFR, CCND1 and MYC in gastric cancer.* BMC Gastroenterol, 2015. **15**: p. 7.
101. Gullo, I., et al., *Minimum biopsy set for HER2 evaluation in gastric and gastro-esophageal junction cancer.* Endoscopy International Open, 2015. **3**(2): p. E165-E170.
102. Huang, S.C., et al., *HER2 testing in paired biopsy and excision specimens of gastric cancer: the reliability of the scoring system and the clinicopathological factors relevant to discordance.* Gastric Cancer, 2016. **19**(1): p. 176-82.
103. Purcell, J.W., et al., *Activity of the Kinesin Spindle Protein Inhibitor Ispinesib (SB-715992) in Models of Breast Cancer.* Clinical Cancer Research, 2010. **16**(2): p. 566.
104. Komlodi-Pasztor, E., D.L. Sackett, and A.T. Fojo, *Inhibitors targeting mitosis: tales of how great drugs against a promising target were brought down by a flawed rationale.* Clin Cancer Res, 2012. **18**(1): p. 51-63.

Tables

Table 1. The summary of treatment regimen.

Table 1

	Patient	Sex	Age (Years)	Stage at pre-treatment	Treatment regimens			
					Initial dosage of treatment	Duration	Initial dosage of treatment	Duration
Trastuzumab	1	M	38	IV	120 mg/day S-1, 60 mg/m^2 cisplatin	5 Weeks × 1	8 mg/kg trastuzumab, 3000 mg/day Capecitabine, 80 mg/m^2 cisplatin	3 Weeks × 1
	2	M	60	IV	8 mg/kg trastuzumab, 3600 mg/day capecitabine, 80 mg/m^2 cisplatin, Investigational agent or placebo ‡	3 Weeks × 4		
	3	M	64	IV	8 mg/kg trastuzumab, 3600 mg/day Capecitabine, 80 mg/m^2 cisplatin, Investigational agent or placebo ‡	3 Weeks × 5		
No trastuzumab	4	M	82	IV	100 mg/day S-1	3 Weeks × 6		
	5	F	58	IIIB	120 mg/day S-1, 35 mg/m^2 docetaxel	4 Weeks × 3		
	6	M	76	IV	120 mg/day S-1, 60 mg/m^2 cisplatin	5 Weeks × 2		

M; Male, F; female

‡; patient 2 and 3 were participants of a clinical study.

Table 2. Changes in human epidermal growth factor receptor 2 (HER2) immunohistochemistry (IHC) score and amplification status after preoperative chemotherapy.

Table 2

			Pre-treatment				Post-treatment			
				Amplification				Amplification		
	Patient	Clinical response (Grade)	HER2 IHC Score	*HER2*	*EGFR*	*MET*	HER2 IHC Score	*HER2*	*EGFR*	*MET*
Trastuzumab	1	2	3	+	-	-	3	+	-	-
	2	1	2	+	-	-	1	-	-	-
	3	2	3	+	-	-	0	-	-	-
No trastuzumab	4	1a	3	+	-	-	0	-	-	-
	5	2	3	+	-	-	0	-	-	-
	6	1b	3	+	-	-	0	-	-	-

M; Male, F; female

‡; patient 2 and 3 were participants of a clinical study.

Figures

Figure 1. Distribution of chromosome number in common cancers.

The data is cited from the reference [4]. The percentage of tumors is plotted against the corresponding chromosome number across various tumor types. Near-diploid chromosome number is the major population in tumors and over triploid chromosome number also has a high percentage. The bracketed numbers indicate the number of tumors analysed for each cancer.

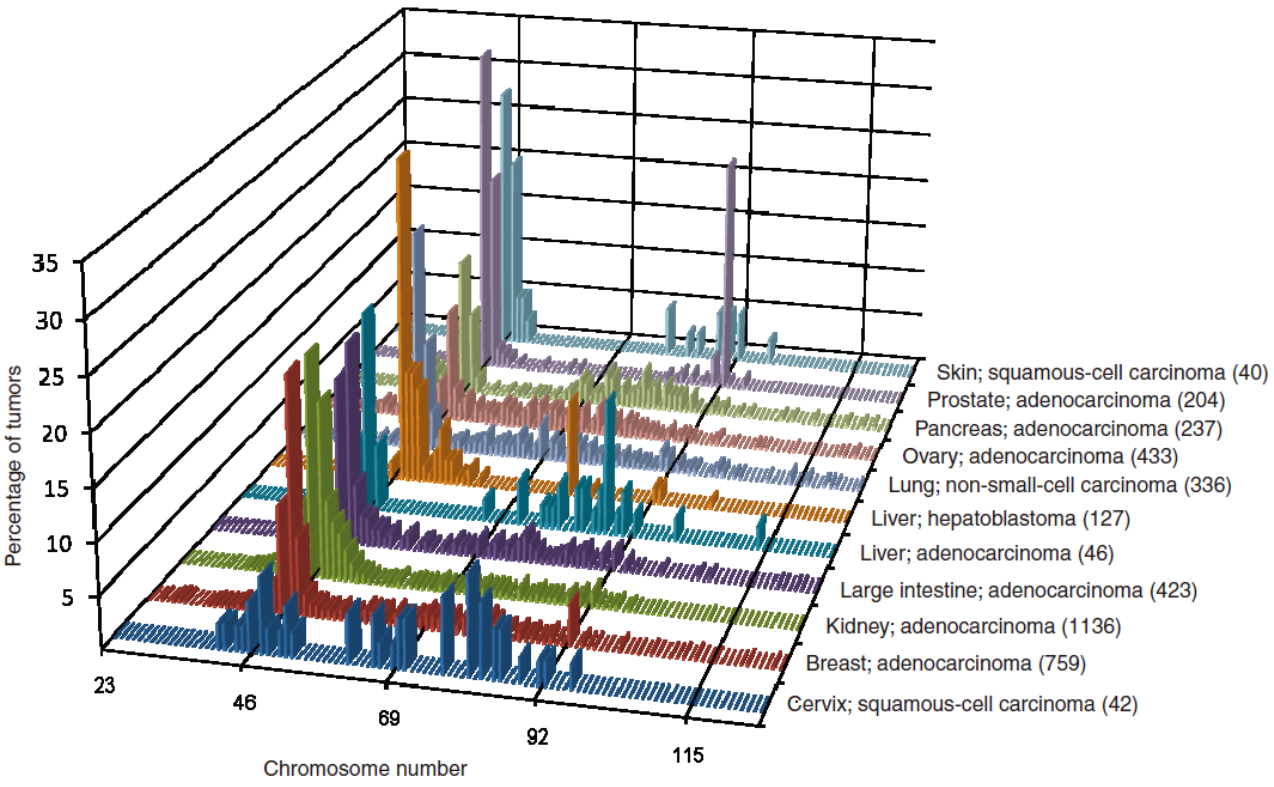
Percentage of tumors
35
30
25
20
15
10
5
23
46
69
92
115
Chromosome number
Skin; squamous-cell carcinoma (40)
Prostate; adenocarcinoma (204)
Pancreas; adenocarcinoma (237)
Ovary; adenocarcinoma (433)
Lung; non-small-cell carcinoma (336)
Liver; hepatoblastoma (127)
Liver; adenocarcinoma (46)
Large intestine; adenocarcinoma (423)
Kidney; adenocarcinoma (1136)
Breast; adenocarcinoma (759)
Cervix; squamous-cell carcinoma (42)

Figure 1

Figure 2. The three main routs to tetraploidy.

The figure is cited from the reference [4]. Cell-cell fusion and cytokinesis failure generate binucleaed tetraploid cells. Mitotic slippage, a state where cells exit mitosis without undergoing anaphase or cytokinesis, generates mononucleated tetraploid cells. 2N, diploid nucleus; 4N, tetraploid nucleus; 4C, diploid nucleus with replicated chromosomes.

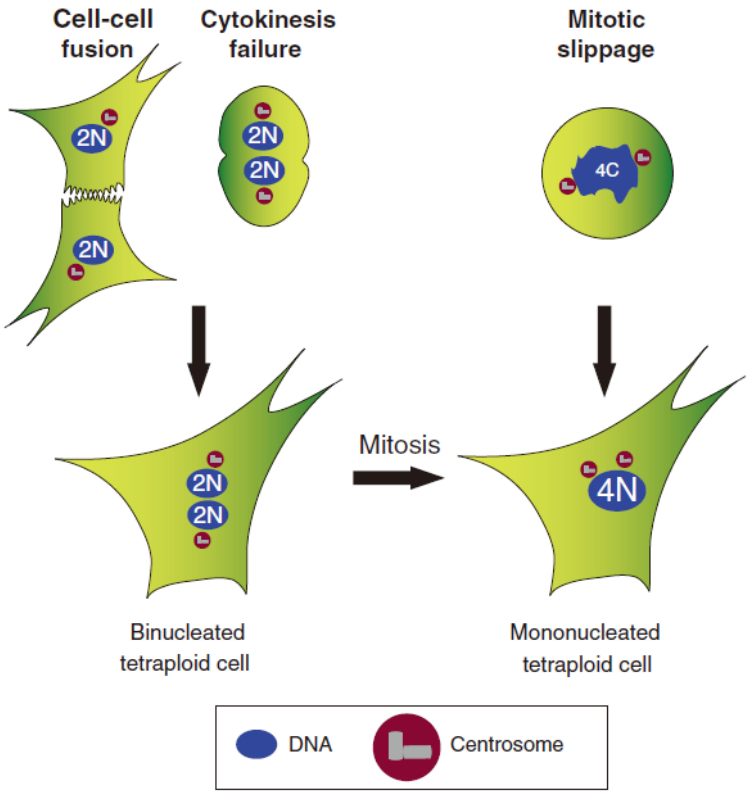
Cell-cell fusion
Cytokinesis failure
Mitotic slippage
2N
2N
2N
4C
Mitosis
2N
2N
4N
Binucleated tetraploid cell
Mononucleated tetraploid cell
DNA
Centrosome

Figure 2

Figure 3. HER family and downstream signalling.

The figure is cited from the reference [17]. HER family is composed of four transmembrane tyrosine kinase receptors: EGFR, HER2, HER3, and HER4. Ligand-binding to the extracellular ligand-binding domain initiates heterodimerization of HER family members. Heterodimerization triggers intracellular signal transduction by activating PI3K/AKT and MAPK pathways, and is involving in regulating cell growth, survival, and apoptosis. AR, amphiregulin; BTC, betacellulin; EPG, epigen; EPR, epiregulin; HB-EFG, heparin-binding EGF-like ligand; NRG, neuregulin.

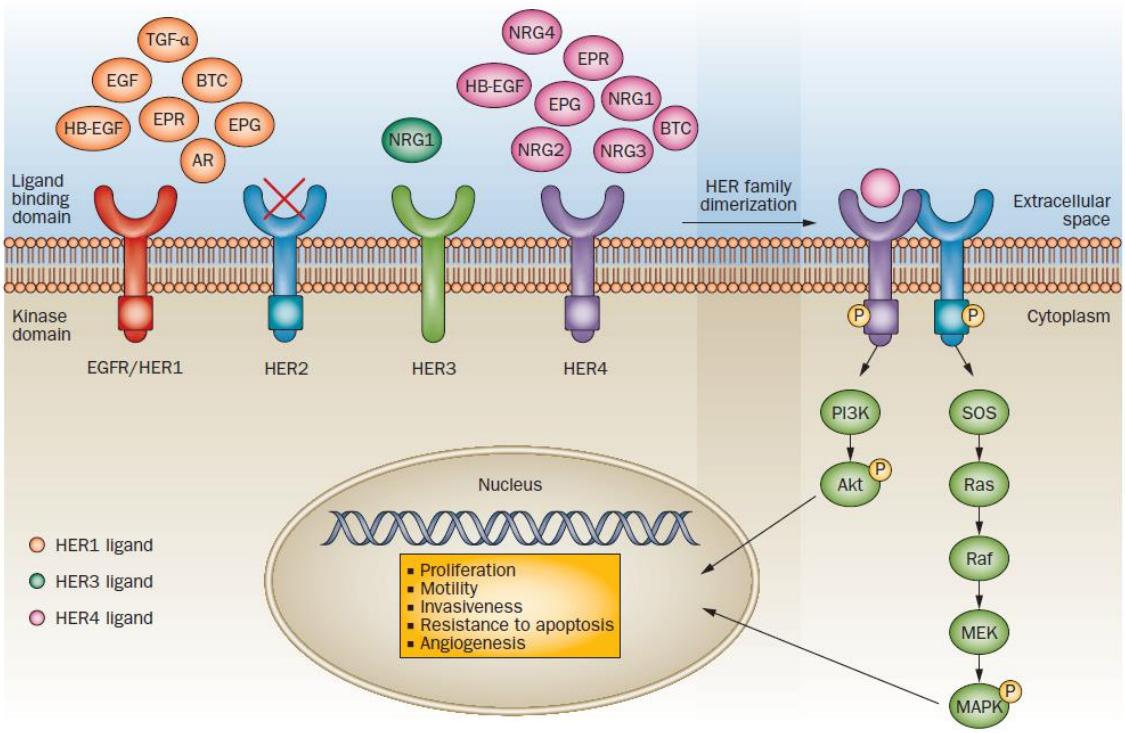
TGF-α
EGF
BTC
HB-EGF
EPR
EPG
AR
NRG4
EPR
HB-EGF
EPG
NRG1
BTC
NRG2
NRG3
NRG1
Ligand binding domain
HER family dimerization
Extracellular space
Kinase domain
Cytoplasm
EGFR/HER1
HER2
HER3
HER4
PI3K
SOS
Akt
Ras
Raf
MEK
MAPK
Nucleus
Proliferation
Motility
Invasiveness
Resistance to apoptosis
Angiogenesis
HER1 ligand
HER3 ligand
HER4 ligand

Figure 3

Figure 4. Eg5 inhibition promotes mitotic division in tetraploid cells.

(A) Selected frames from live-cell imaging of representative HeLa Fucci2 cells treated with hesperadin. Hesperadin treatment rapidly induced mitotic slippage, resulting in the generation of tetraploid cells. Scale bar, 10 μm. **(B)** Schemes of the experiments shown in Figure 4**C–F**. **(C, D)** The anti-proliferative effects of anti-mitotic agents were quantified by crystal violet staining. Cells were fixed at 48 h after treatment with anti-mitotic agents as shown in Figure 4**B**. Data are means ± s.d. (n=3). ***p < 0.0001, NS; not significant. Representative images of crystal violet staining are shown in **C**. **(E)** Tetraploid and non-tetraploid HeLa Fucci2 cells underwent live-cell imaging analysis. After treatment with anti-mitotic agents as shown in **B**, the duration of the first mitosis was measured, from cell rounding up to re-attachment or death. Red lines, median; blue bars, interquartile range (n ≥ 59). **p < 0.001, ***p<0.0001. **(F)** Cell behaviours during the first mitosis after treatment with anti-mitotic agents were examined by live-cell imaging analysis (n ≥ 45). **(G)** Schemes of the experiments shown in Figure 4**H, I**. **(H, I)** Quantification of mitotic spindle polarity in tetraploid and non-tetraploid HeLa cells. Cells were fixed and co-stained with the indicated antibodies. Representative images are shown in **H**. Data are means ± s.d. from three independent experiments (≥ 250 cells per experiment). **p < 0.001. Scale bar, 10 μm.

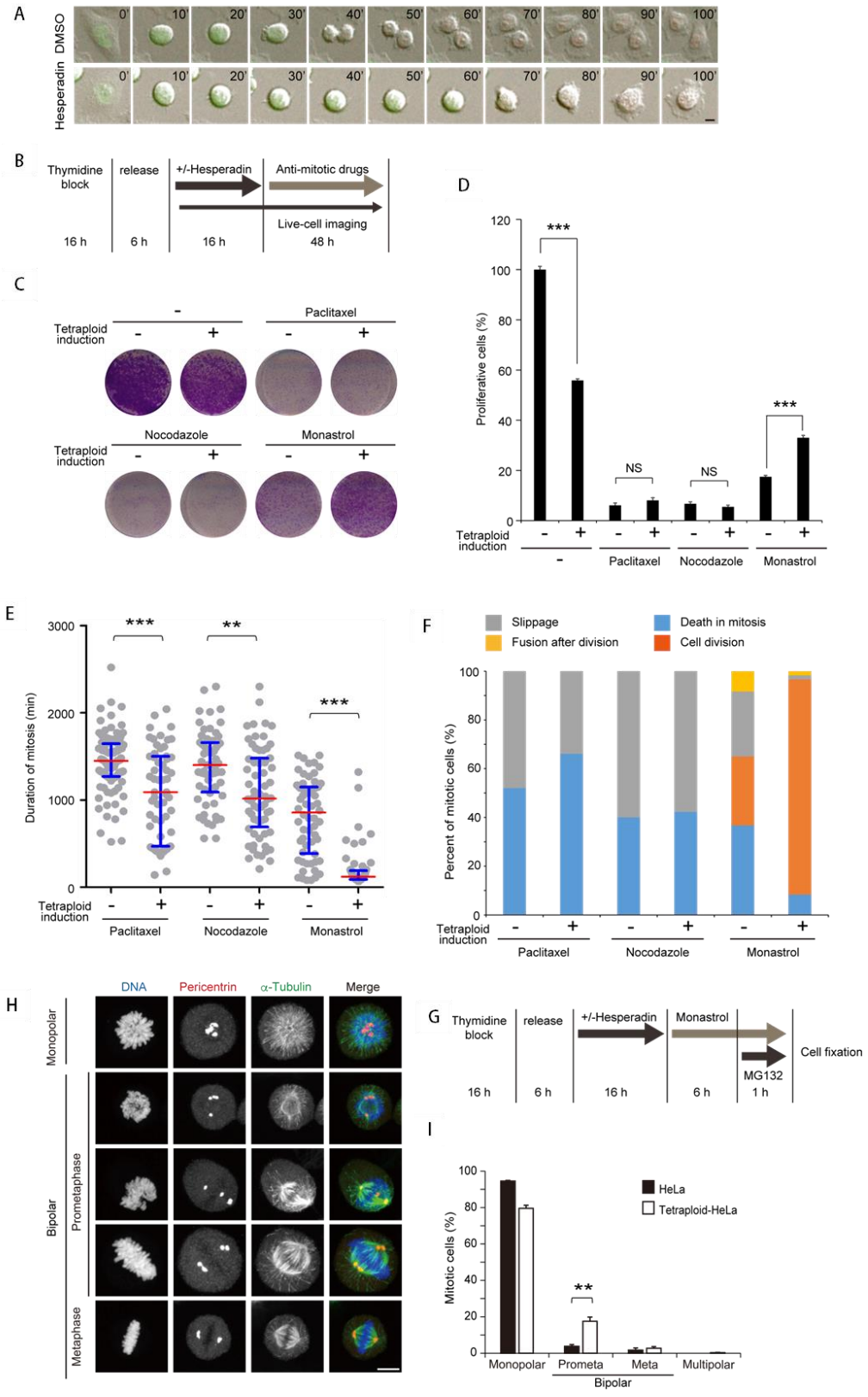
A
DMSO
Hesperadin
0'
10'
20'
30'
40'
50'
60'
70'
80'
90'
100'
B
Thymidine block
release
+/-Hesperadin
Anti-mitotic drugs
Live-cell imaging
16 h
6 h
16 h
48 h
C
Tetraploid induction
Paclitaxel
Nocodazole
Monastrol
D
Proliferative cells (%)
***
NS
NS
***
Tetraploid induction
Paclitaxel
Nocodazole
Monastrol
E
Duration of mitosis (min)
***
**
***
Tetraploid induction
Paclitaxel
Nocodazole
Monastrol
F
Slippage
Fusion after division
Death in mitosis
Cell division
Percent of mitotic cells (%)
Tetraploid induction
Paclitaxel
Nocodazole
Monastrol
G
Thymidine block
release
+/-Hesperadin
Monastrol
MG132
Cell fixation
16 h
6 h
16 h
6 h
1 h
H
DNA
Pericentrin
α-Tubulin
Merge
Monopolar
Bipolar
Prometaphase
Metaphase
I
Mitotic cells (%)
HeLa
Tetraploid-HeLa
**
Monopolar
Prometa
Meta
Multipolar
Bipolar

Figure 4

Figure 5. Eg5 regulates spindle polarity and cell division in tetraploid cells.

(A) Schemes of the experiments shown in Figure 5**B, C**. **(B, C)** Quantification of mitotic spindle polarity during anaphase and telophase in HeLa cells. Cells were fixed and co-stained with the indicated antibodies. Representative images of mitotic cells displaying missegregation are shown in **B**. Data are means ± s.d. from three independent experiments (≥ 150 cells per experiment). Scale bar, 10 μm.

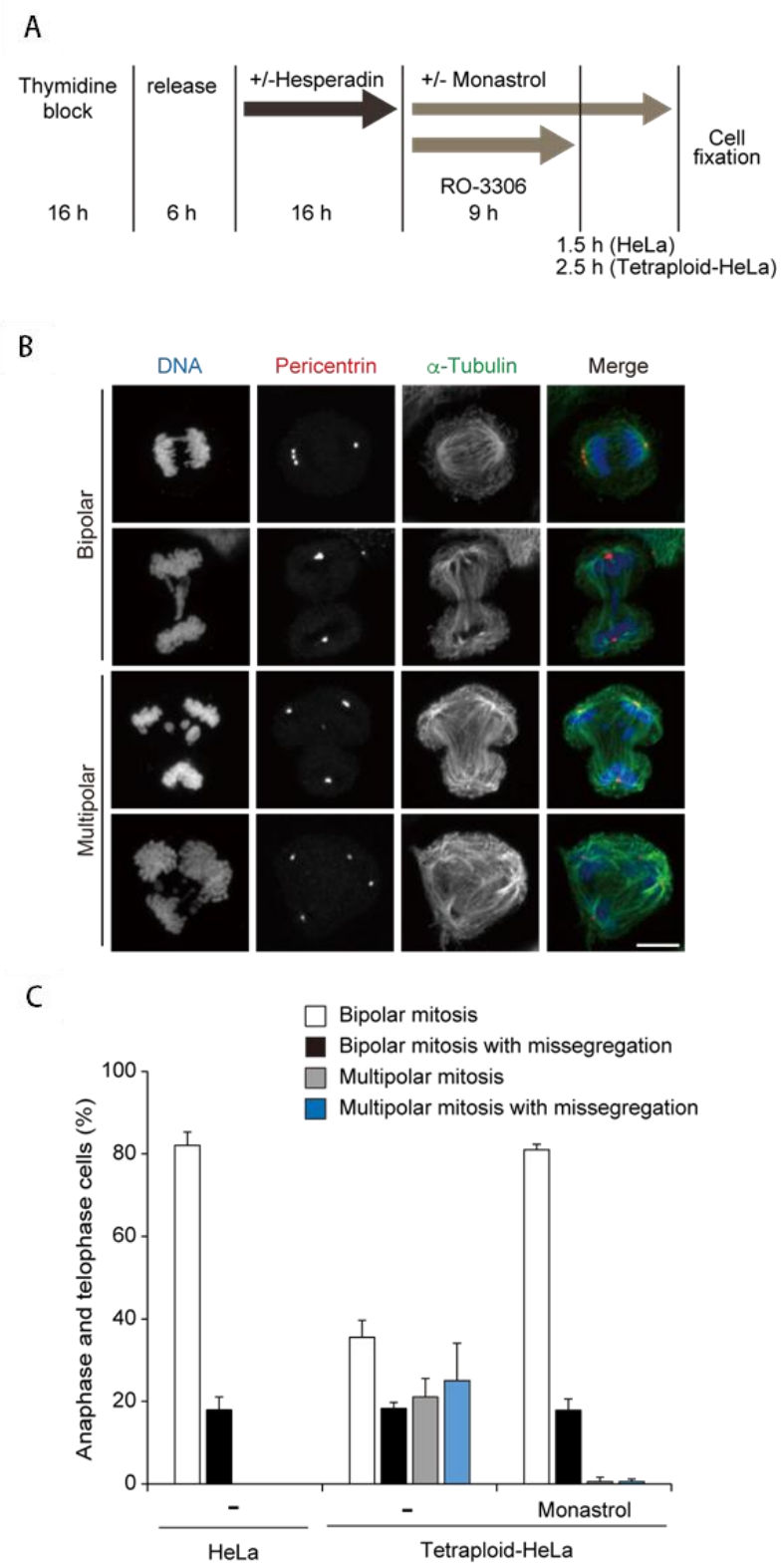
A
Thymidine block
release
+/-Hesperadin
+/- Monastrol
Cell fixation
RO-3306
16 h
6 h
16 h
9 h
1.5 h (HeLa)
2.5 h (Tetraploid-HeLa)
B
DNA
Pericentrin
α-Tubulin
Merge
Bipolar
Multipolar
C
Bipolar mitosis
Bipolar mitosis with missegregation
Multipolar mitosis
Multipolar mitosis with missegregation
Anaphase and telophase cells (%)
100
80
60
40
20
0
-
-
Monastrol
HeLa
Tetraploid-HeLa

Figure 5

Figure 6. The relationship between the level of phospho-Eg5 localised at the spindle and spindle polarity in tetraploid cells.

(A) Schemes of the experiments shown in Figure 6**B, C. (B, C)** Quantification of spindle polarity in tetraploid HeLa and HCT116 $p53^{-/-}$ cells. Cells were fixed and co-stained with the indicated antibodies. Representative images of tetraploid HeLa cells are shown in **B**. Data are means ± s.d. from three independent experiments (≥ 250 cells per experiment). *$p < 0.0001$. Scale bar, 10 μm. **(D)** Schemes of the experiments shown in Figure 6**E–I**. **(E-I)** Cells were synchronised by a thymidine block for 16 h (TB) and then treated with RO-3306 for 4 h. Mitotic cells were collected by mitotic shake-off after MG132 treatment for 2 h (shake-off). Immunoblot analysis in **E** was performed using the indicated antibodies. Phospho-histone H3 (Ser10) was monitored as a mitosis-specific marker (pH3S10). Levels of Eg5, normalized against β-actin, are shown relative to HeLa mitotic shake-off (defined as 1). **(F)** Quantification of the relative ratio of phospho-Eg5 to Eg5 in cells subjected to mitotic shake-off. Data are means ± s.d. from three independent experiments. **(G)** Representative immunofluorescence images showing the localisation of phospho-Eg5. Cells were fixed and co-stained with the indicated antibodies. Scale bar, 10 μm. **(H)** Line graphs of the fluorescence intensities of phospho-Eg5 and γ-tubulin staining from representative images of metaphase cells shown in **G**. **(I)** Quantification of fluorescence intensity of phospho-Eg5. Open circles represent individual cells (n≥ 20).

Red lines, medians; blue bars, interquartile range. A.U., arbitrary units. **p < 0.0001.

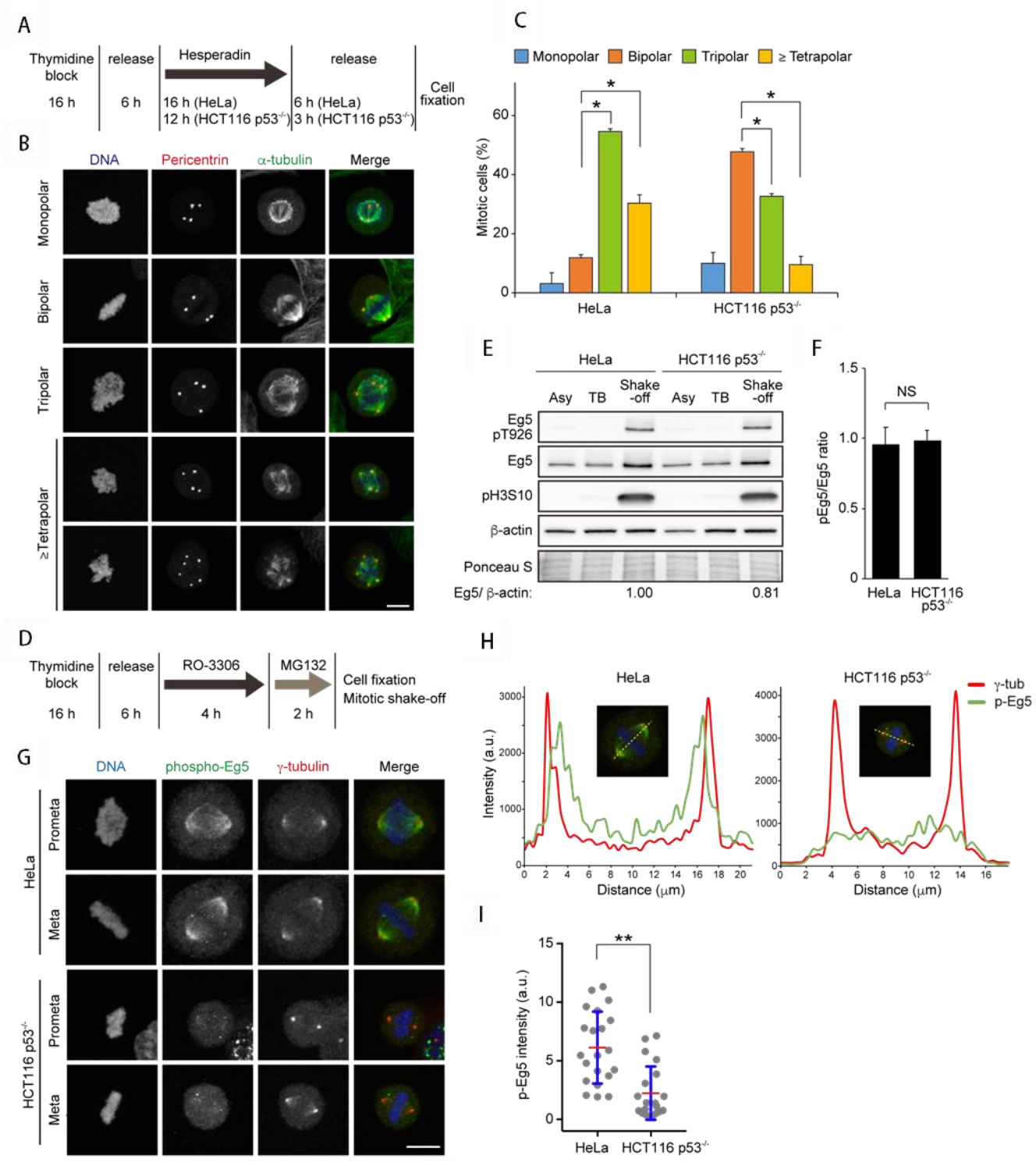
A
Thymidine block
16 h
release
6 h
Hesperadin
16 h (HeLa)
12 h (HCT116 p53-/-)
release
6 h (HeLa)
3 h (HCT116 p53-/-)
Cell fixation
B
DNA
Pericentrin
α-tubulin
Merge
Monopolar
Bipolar
Tripolar
≥Tetrapolar
C
Monopolar
Bipolar
Tripolar
≥ Tetrapolar
Mitotic cells (%)
HeLa
HCT116 p53-/-
D
Thymidine block
16 h
release
6 h
RO-3306
4 h
MG132
2 h
Cell fixation
Mitotic shake-off
E
HeLa
HCT116 p53-/-
Asy
TB
Shake -off
Eg5 pT926
Eg5
pH3S10
β-actin
Ponceau S
Eg5/ β-actin:
1.00
0.81
F
NS
pEg5/Eg5 ratio
HeLa
HCT116 p53-/-
G
DNA
phospho-Eg5
γ-tubulin
Merge
HeLa
Prometa
Meta
HCT116 p53-/-
Prometa
Meta
H
HeLa
HCT116 p53-/-
γ-tub
p-Eg5
Intensity (a.u.)
Distance (μm)
I
p-Eg5 intensity (a.u.)
HeLa
HCT116 p53-/-

Figure 6

Figure 7. Effect of forced changes in the level of phospho-Eg5 localised at the spindle on spindle polarity in tetraploid cells.

(A–F) HeLa and HCT116 $p53^{-/-}$ cells were transfected with a mock control IRES-GFP plasmid (mock) or that harbouring Myc-$Eg5^{WT}$ or Myc-$Eg5^{T926A}$ at 24 h before a single thymidine block. This was followed by tetraploid induction and release, as shown in Figure 6**A**. Thereafter, cells were collected for immunoblot analysis or fixed for immunofluorescence staining. **(A)** Immunoblot analysis was performed using the indicated antibodies. **(B)** Tetraploid HeLa cells were fixed and co-stained with the indicated antibodies. Representative images are shown. **(C)** Quantification of mitotic spindle polarity in tetraploid HeLa cells expressing the indicated plasmids, as determined by co-staining cells with anti-α-tubulin, pericentrin, and Myc antibodies, as well as DAPI. Only GFP-positive cells were counted. Data are means ± s.d. from three independent experiments (≥ 80 cells per experiment for mock control, ≥ 150 cells per experiment for Myc-$Eg5^{WT}$ and Myc-$Eg5^{T926A}$). **(D)** Diploid and tetraploid HCT116 $p53^{-/-}$ cells were collected and immunoblot analysis was performed using the indicated antibodies. **(E)** Tetraploid HCT116 $p53^{-/-}$ cells were fixed and co-stained with the indicated antibodies. Representative images are shown. **(F)** Quantification of mitotic spindle polarity in diploid and tetraploid HCT116 $p53^{-/-}$ cells expressing the indicated plasmids, as determined by co-staining cells with an anti-α-tubulin, pericentrin, and Myc antibody and DAPI. Only

GFP-positive cells were counted. Data are means ± s.d. from three independent experiments (≥ 200 diploid cells per experiment, ≥ 250 tetraploid cells per experiment for mock control, ≥ 94 tetraploid cells per experiment for Myc-Eg5^{WT}). *$p < 0.05$, **$p < 0.001$, NS; not significant. Scale bar, 10 μm.

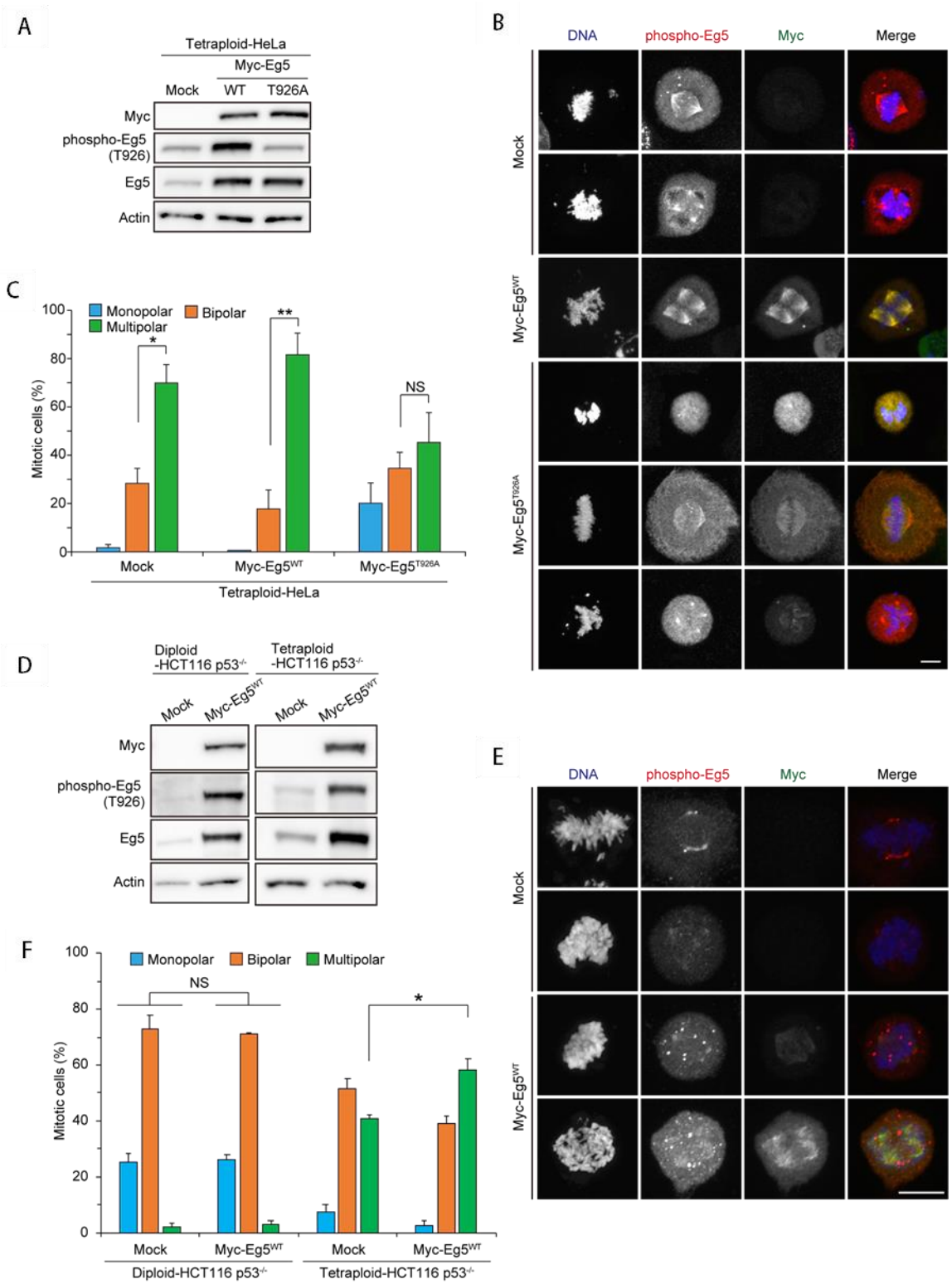
A
Tetraploid-HeLa
Myc-Eg5
Mock
WT
T926A
Myc
phospho-Eg5 (T926)
Eg5
Actin
B
DNA
phospho-Eg5
Myc
Merge
Mock
Myc-Eg5WT
Myc-Eg5T926A
C
Monopolar
Bipolar
Multipolar
Mitotic cells (%)
*
**
NS
Mock
Myc-Eg5WT
Myc-Eg5T926A
Tetraploid-HeLa
D
Diploid -HCT116 p53-/-
Tetraploid -HCT116 p53-/-
Mock
Myc-Eg5WT
Myc
phospho-Eg5 (T926)
Eg5
Actin
E
DNA
phospho-Eg5
Myc
Merge
Mock
Myc-Eg5WT
F
Monopolar
Bipolar
Multipolar
Mitotic cells (%)
NS
*
Mock
Myc-Eg5WT
Diploid-HCT116 p53-/-
Tetraploid-HCT116 p53-/-

Figure 7

Figure 8. Involvement of Kif15 and HSET in spindle polarity in tetraploid cells.

(A, B) HeLa cells were transfected with the indicated siRNAs. After 12 h, cells were synchronized by a single thymidine block followed by tetraploid induction and release, as shown in Figure 6**A**. **(A)** Immunoblot analysis was performed using the indicated antibodies. **(B)** Tetraploid HeLa cells were fixed and co-stained with anti-α-tubulin and pericentrin antibodies, as well as DAPI. **(C, D)** HeLa cells were transfected with mock control plasmid (mock) or plasmid harbouring Myc-Kif15 12 h before a single thymidine block, followed by tetraploid induction as shown in Figure 6**A** and release into *S*-trityl-*L*-cysteine. Thereafter, cells were collected for immunoblot analysis or fixed for immunofluorescence staining. **(C)** Immunoblot analysis was performed using the indicated antibodies. **(D)** Tetraploid HeLa cells were fixed and co-stained with anti-Myc, α-tubulin, and pericentrin antibodies, as well as DAPI. Only Myc-positive cells were counted. **(E, F)** HCT116 $p53^{-/-}$ cells were transfected with mock control plasmid (mock) or plasmid harbouring Myc-Kif15 12 h before a single thymidine block followed by tetraploid induction and release, as shown in Figure 6**A**. Thereafter, cells were collected for immunoblot analysis or fixed for immunofluorescence staining. Immunoblot analysis was performed using the antibodies indicated in **E**. Tetraploid HCT116 $p53^{-/-}$ cells were fixed and co-stained with anti-Myc, α-tubulin, and pericentrin antibodies, as well as

DAPI. Only Myc-positive cells were counted in **F**. **(G, H)** HeLa cells were transfected with mock control IRES-GFP plasmid (mock) or plasmid harbouring HSET at 12 h before a single thymidine block followed by tetraploid induction and release, as shown in Figure 6**A**. Thereafter, cells were collected for immunoblot analysis or fixed for immunofluorescence staining. **(G)** Immunoblot analysis was performed using the indicated antibodies. **(H)** Tetraploid HeLa cells were fixed and co-stained with an anti-α-tubulin and pericentrin antibodies, as well as DAPI. Only GFP-positive cells were counted. Data are means ± s.d. from three independent experiments (≥ 150 cells per experiment for **D** and **H**, ≥ 250 cells per experiment for **B** and **F)**. *$p < 0.01$, **$p = 0.0002$, ***$p < 0.0001$, NS; not significant.

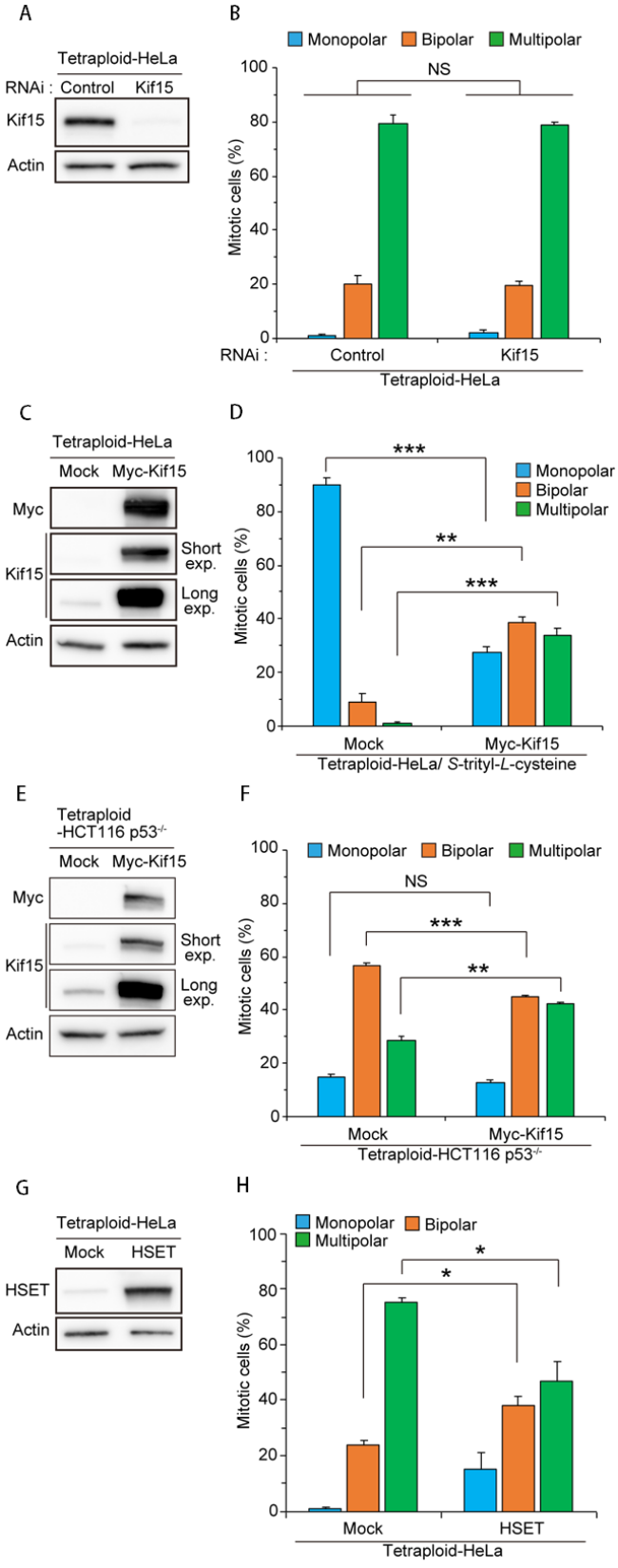
A
Tetraploid-HeLa
RNAi : Control Kif15
Kif15
Actin
B
Monopolar Bipolar Multipolar
NS
Mitotic cells (%)
RNAi : Control Kif15
Tetraploid-HeLa
C
Tetraploid-HeLa
Mock Myc-Kif15
Myc
Kif15
Short exp.
Long exp.
Actin
D
Monopolar
Bipolar
Multipolar
***
**
***
Mitotic cells (%)
Mock Myc-Kif15
Tetraploid-HeLa/ S-trityl-L-cysteine
E
Tetraploid -HCT116 p53-/-
Mock Myc-Kif15
Myc
Kif15
Short exp.
Long exp.
Actin
F
Monopolar Bipolar Multipolar
NS
***
**
Mitotic cells (%)
Mock Myc-Kif15
Tetraploid-HCT116 p53-/-
G
Tetraploid-HeLa
Mock HSET
HSET
Actin
H
Monopolar Bipolar
Multipolar
*
*
Mitotic cells (%)
Mock HSET
Tetraploid-HeLa

Figure 8

Figure 9. Generation of aneuploid cells from tetraploid cells in an Eg5 activity-dependent manner.

(A–C) DNA content analysis of populations derived from tetraploid cells. HeLa and HCT116 $p53^{-/-}$ cells were synchronised by a single thymidine block for 16 h, released for 6 h, treated with hesperadin for 16 h (HeLa) or 12 h (HCT116 $p53^{-/-}$) and then cultured in fresh medium containing monastrol or DMSO. Cells were collected 7 days after the medium change, stained with propidium iodide and analysed by flow cytometry. Results obtained in the absence of monastrol are shown in **A**. Quantification of cells with an approximately 2N DNA content after 7 days of culture in the absence of monastrol is shown in **B**. Data are means + s.d. from three independent experiments. *p = 0.0001 by the unpaired *t*-test. Results obtained in the presence of monastrol are shown in **C. (D, E)** FISH analysis of tetraploid HeLa using probes against centromeric DNA of chromosome 6 (green) and chromosome 18 (orange) was performed after 7 days of culture as described above. Representative images of FISH analysis are shown in **D**. The percentages of cells with the indicated number of signals are shown in **E**. **(F, G)** FISH analysis of tetraploid HCT116 $p53^{-/-}$ cells. Scale bar, 10 μm. Data are means + s.d. from three independent experiments (≥ 215 cells per experiment). **(H)** Representative images of immunohistochemical staining to detect Eg5 in gastric tumors of different histological grades. The boundary between grades 1 and 2 was chosen as the cutoff point for high or

low Eg5 expression. Scale bar, 50 μm. **(I)** Correlation analysis between Eg5 expression and DNA ploidy in gastric tumor specimens. DNA ploidy status was determined using the DNA index (DI) score described in the 'Methods' section.

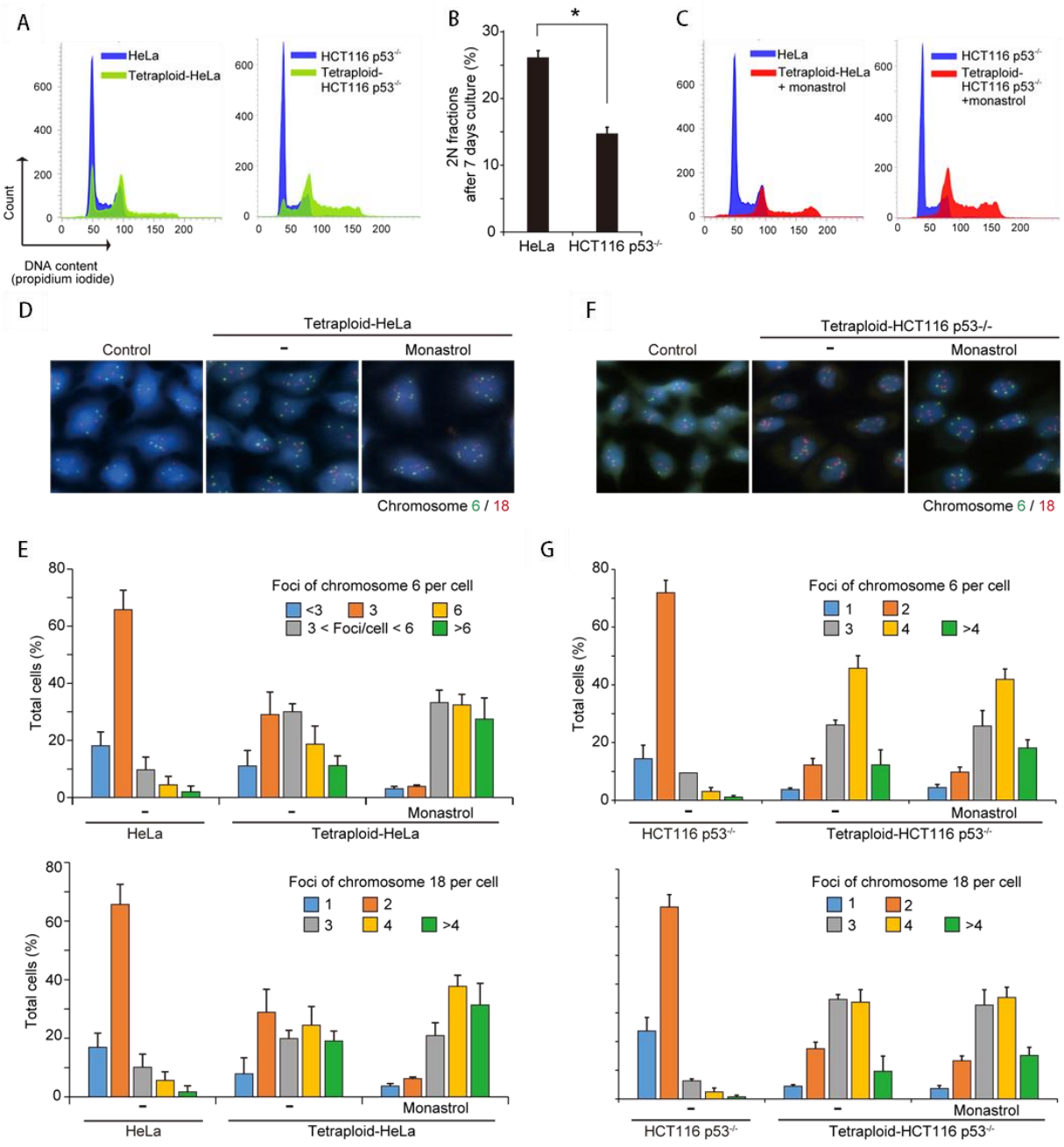
A
HeLa
Tetraploid-HeLa
HCT116 p53-/-
Tetraploid-HCT116 p53-/-
Count
DNA content (propidium iodide)
B
2N fractions after 7 days culture (%)
HeLa
HCT116 p53-/-
C
HeLa
Tetraploid-HeLa + monastrol
HCT116 p53-/-
Tetraploid-HCT116 p53-/- +monastrol
D
Tetraploid-HeLa
Control
-
Monastrol
Chromosome 6 / 18
F
Tetraploid-HCT116 p53-/-
Control
-
Monastrol
Chromosome 6 / 18
E
Foci of chromosome 6 per cell
<3
3
6
3 < Foci/cell < 6
>6
Total cells (%)
Monastrol
HeLa
Tetraploid-HeLa
Foci of chromosome 18 per cell
1
2
3
4
>4
G
Foci of chromosome 6 per cell
Foci of chromosome 18 per cell
HCT116 p53-/-
Tetraploid-HCT116 p53-/-

Figure 9

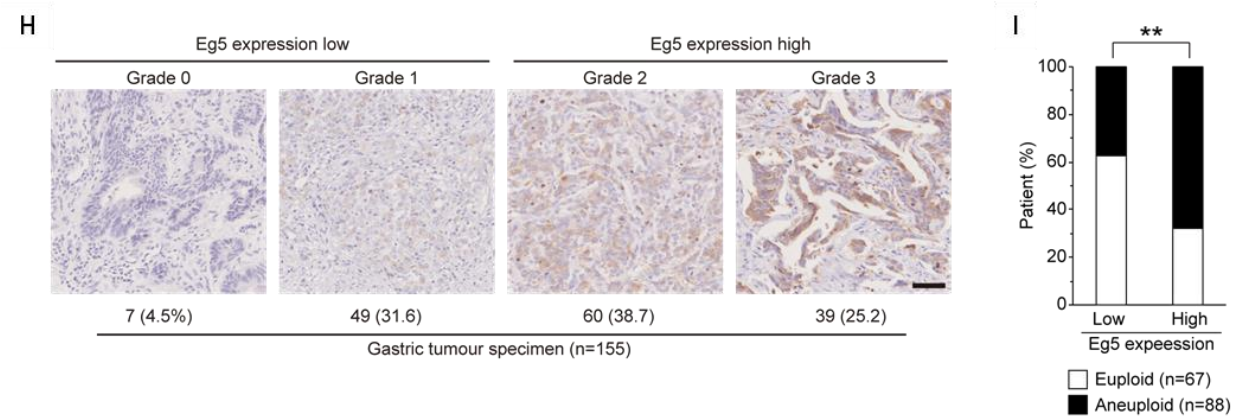
H
Eg5 expression low
Eg5 expression high
Grade 0
Grade 1
Grade 2
Grade 3
7 (4.5%)
49 (31.6)
60 (38.7)
39 (25.2)
Gastric tumour specimen (n=155)
I
**
Patient (%)
100
80
60
40
20
0
Low
High
Eg5 expeession
Euploid (n=67)
Aneuploid (n=88)

Figure 9

Figure 10. A model for Eg5-dependent mitotic regulation in tetraploid cells.

Tetraploid cells, which can arise via multiple mechanisms, have two pairs of centrosomes in G2 and mitotic phases, and can therefore undergo multipolar or bipolar mitosis. When the forces among kinesins are counterbalanced, tetraploid cells preferentially undergo bipolar division, which maintains tetraploidy. When the level of functional Eg5 is high, tetraploid cells undergo multipolar division, resulting in heterogenous aneuploid progenies with near-diploid DNA contents.

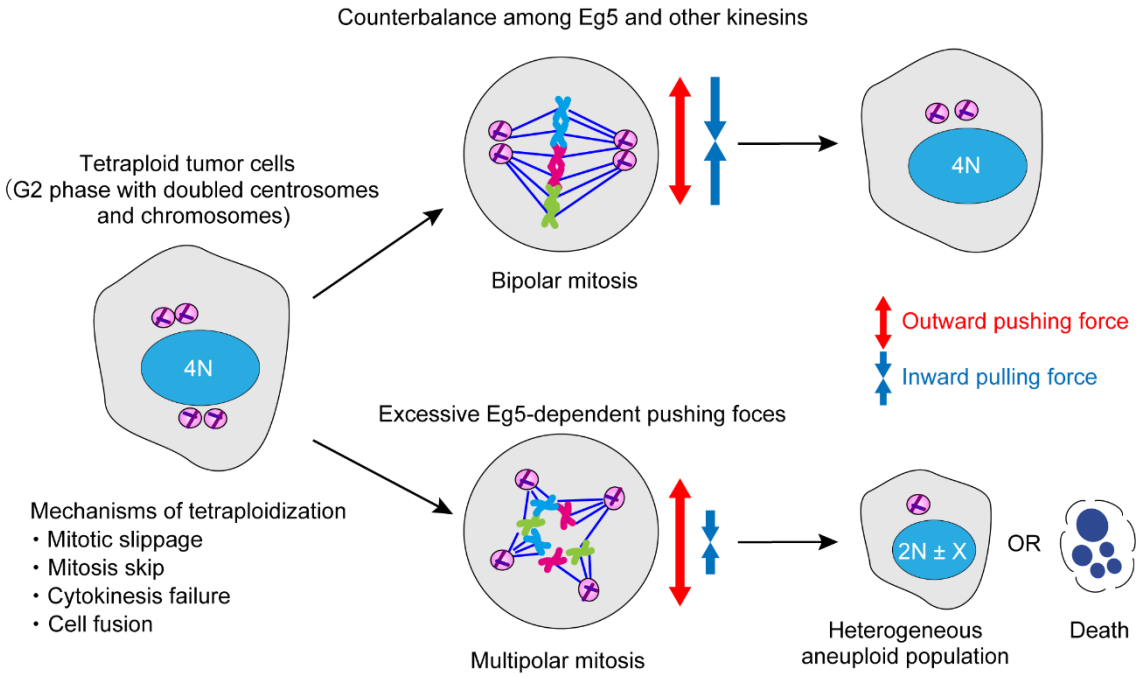
Counterbalance among Eg5 and other kinesins
Tetraploid tumor cells
(G2 phase with doubled centrosomes
and chromosomes)
4N
Bipolar mitosis
4N
Outward pushing force
Inward pulling force
Excessive Eg5-dependent pushing foces
Mechanisms of tetraploidization
• Mitotic slippage
• Mitosis skip
• Cytokinesis failure
• Cell fusion
Multipolar mitosis
2N ± X
OR
Heterogeneous
aneuploid population
Death

Figure 10

Figure 11. Immunohistochemical (IHC) staining of human epidermal growth factor receptor 2 (HER2), and fluorescence in situ hybridization (FISH) of epidermal growth factor receptor (EGFR)/hepatocyte growth factor receptor (MET)/HER2 in a case that received trastuzumab in combination with preoperative chemotherapy (patient 1 in Table 1 and 2).

(A-D) Pre-treatment biopsy specimen. **(E-K)** Post-treatment surgical resected specimen from the same patient. **(A, B, E, F, I)** HER2 IHC staining (magnification: A; ×3, B, F, I; ×60, E; ×2.5). **(C, G, J)** Hematoxylin and eosin staining (magnification: ×60). **(D, H, K)** FISH signals of *EGFR/MET/HER2* (magnification: ×500). FISH was performed with a probe for EGFR/MET/HER2 in the same region as HER2 IHC staining. *EGFR, MET* and *HER2* gene signals are represented as blue, red, and green, respectively. HER2 IHC score was 3+ in pre- and post-treatment specimens. *HER2* amplification was observed in the same region as HER2 IHC staining, whereas no *EGFR* or *MET* amplification was observed.

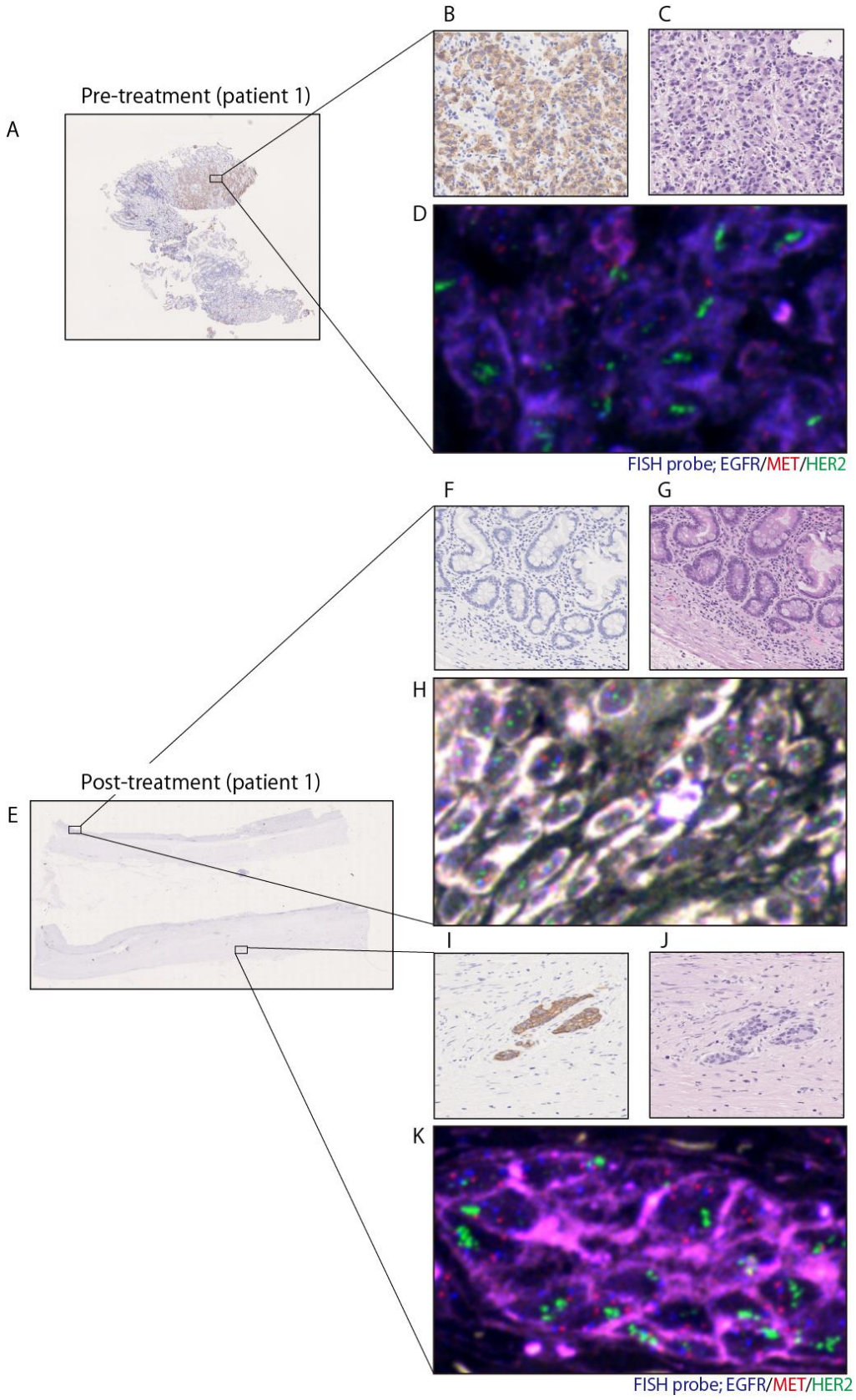
A
Pre-treatment (patient 1)
B
C
D
FISH probe; EGFR/MET/HER2
E
Post-treatment (patient 1)
F
G
H
I
J
K
FISH probe; EGFR/MET/HER2

Figure 11

Figure 12. Immunohistochemical (IHC) staining of human epidermal growth factor receptor 2 (HER2), and fluorescence in situ hybridization (FISH) of epidermal growth factor receptor (EGFR)/hepatocyte growth factor receptor (MET)/HER2 in a case that received cytotoxic preoperative chemotherapy (patient 6 in Table 1 and 2).

(A-G) Pre-treatment biopsy specimen. **(H-K)** Post-treatment surgical resected specimen from the same patient. **(A, B, E, H, I)** HER2 IHC staining (magnification: A; ×3, B, E, I; ×100, H; ×2.5). **(C, F, J)** Hematoxylin and eosin staining (magnification: ×100). **(D, G, K)** FISH signals of *EGFR/MET/HER2* (magnification: ×500). FISH was performed with a probe for *EGFR/MET/HER2* in the same region as HER2 IHC staining. *EGFR, MET* and *HER2* gene signals are represented as blue, red, and green, respectively. HER2 IHC score was 3+ in the pre-treatment specimen and 0 in the post-treatment specimen. *HER2* amplification was observed in the same region as HER2 IHC staining, whereas no *EGFR* or *MET* amplification was observed.

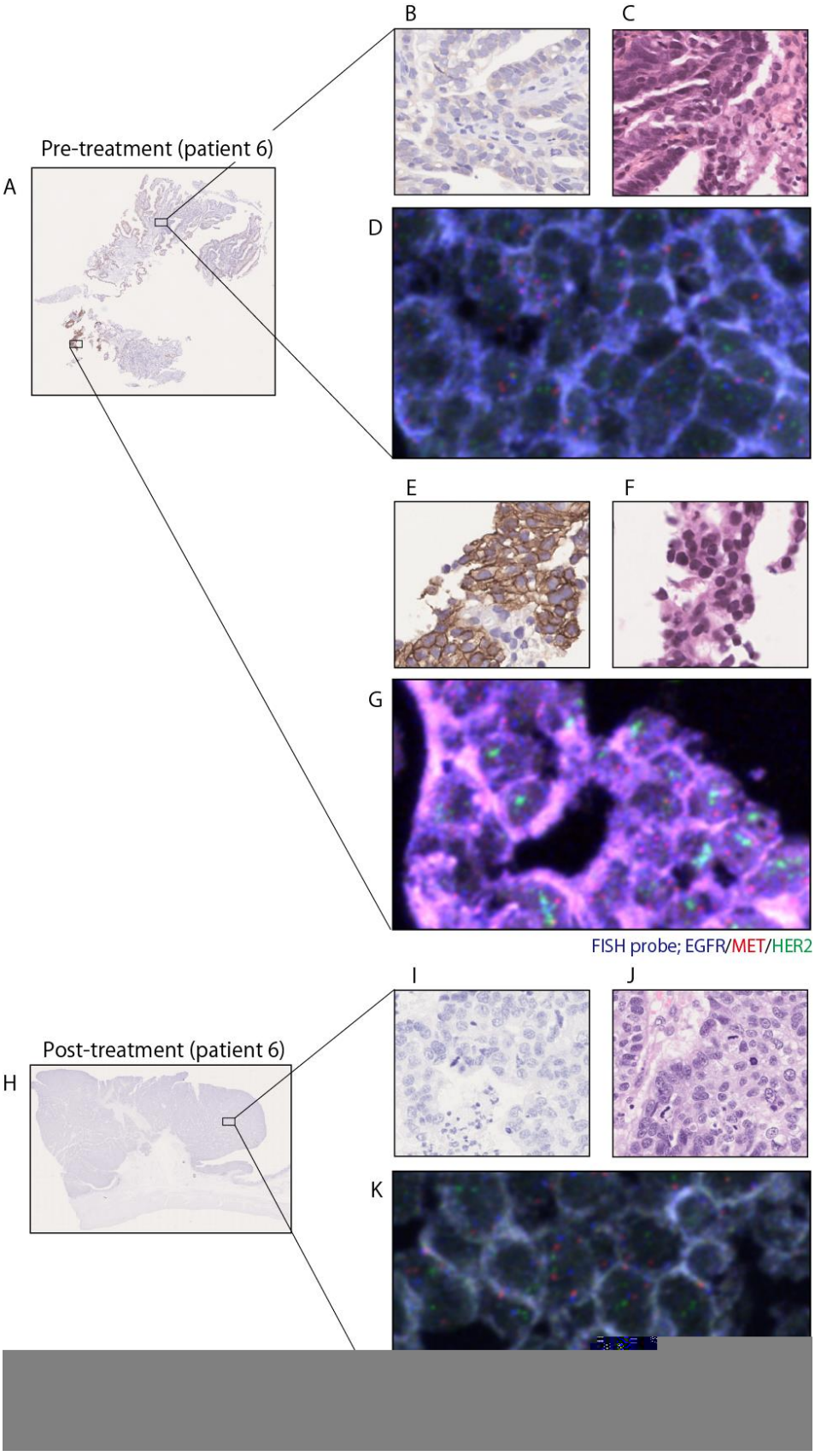
B
C
Pre-treatment (patient 6)
A
D
E
F
G
FISH probe; EGFR/MET/HER2
I
J
Post-treatment (patient 6)
H
K

Figure 12

Figure 13. A scheme of intra-tumoral heterogeneity of HER2 expression and acquired drug resistance.

Intra-tumoral heterogeneous HER2 expression supposedly leads to loss of HER2-positive cells and accumulation of HER2-negative cells by anti-tumor therapy treatment. The loss of target molecules results in acquired resistance to the continuous targeted therapy.

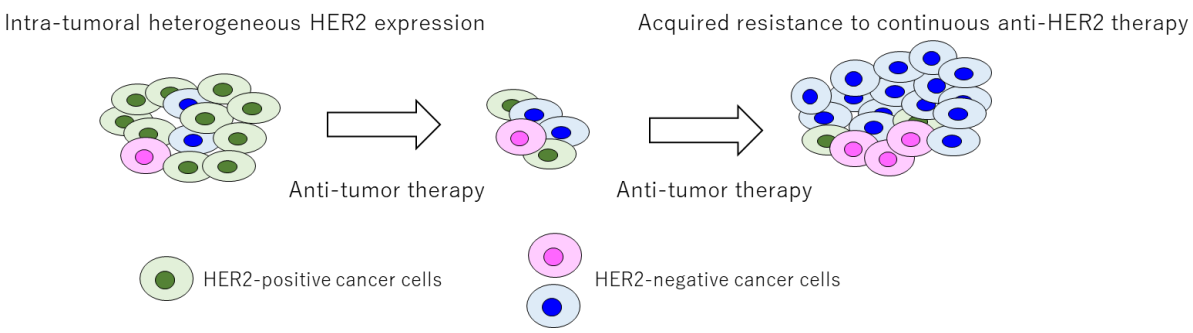
Intra-tumoral heterogeneous HER2 expression
Acquired resistance to continuous anti-HER2 therapy
Anti-tumor therapy
Anti-tumor therapy
HER2-positive cancer cells
HER2-negative cancer cells

Figure 13